

THREE TIME-SCALES IN AN EXTENDED BONHOEFFER-VAN DER POL OSCILLATOR

P. DE MAESSCHALCK, E. KUTAFINA, AND N. POPOVIĆ

ABSTRACT. We consider an extended three-dimensional Bonhoeffer-van der Pol oscillator which generalises the planar FitzHugh-Nagumo model from mathematical neuroscience, and which was recently studied by Sekikawa *et al.* [18] and by Freire and Gallas [7]. Focussing on a parameter regime which has hitherto been neglected, and in which the governing equations evolve on three distinct time-scales, we propose a reduction to a model problem that was formulated by Krupa *et al.* [12] as a canonical form for such systems. Based on results previously obtained in [12], we characterise completely the mixed-mode dynamics of the resulting three time-scale extended Bonhoeffer-van der Pol oscillator from the point of view of geometric singular perturbation theory, thus complementing the findings reported in [18]. In particular, we specify in detail the mixed-mode patterns that are observed upon variation of a bifurcation parameter which is naturally obtained by combining two of the original parameters in the system, and we derive asymptotic estimates for the corresponding parameter intervals. We thereby also disprove a conjecture of [22], where it was postulated that no stable periodic orbits of mixed-mode type can be observed in an equivalent extension of the Bonhoeffer-van der Pol equations.

1. INTRODUCTION

In this article, we consider the three-dimensional Bonhoeffer-van der Pol oscillator, a known extension of the classical planar FitzHugh-Nagumo equations from mathematical neuroscience [9], which was studied most recently by Sekikawa *et al.* [18] and by Freire and Gallas [7]. Specifically, we are concerned with the following system of equations:

$$\begin{aligned} (1a) \quad & \varepsilon \dot{x} = x(1 - x^2) + y + z, \\ (1b) \quad & \dot{y} = -x - k_1 y + B_0, \\ (1c) \quad & \dot{z} = k_3(-x - k_1 z + B_0); \end{aligned}$$

here, we have retained the notation of [18], with ε the ‘small’ singular perturbation parameter and three additional parameters which are denoted by B_0 , k_1 , and k_3 .

Equation (1) is known to display rich dynamics on at least two different time-scales due to the presence of the small parameter ε [18, 7]. Here, we focus on the stable mixed-mode oscillatory behaviour [3] that was reported both numerically and experimentally – by construction of an equivalent electrical circuit – in [18]; in the follow-up article [7], the resulting mixed-mode patterns were organised systematically in terms of Farey trees, as well as of more general Stern-Brocot trees. In both studies, the two parameters B_0 and k_3 were identified as crucial for the unfolding of the bifurcation structure of (1); in particular, Sekikawa *et al.* [18] observed mixed-mode dynamics close to a pair of (supercritical) Hopf bifurcations which occur in (1) for $B_0 \approx \pm \frac{1}{2}$, where, additionally, k_3 was assumed to be close to one. (We note that there is a symmetry $(x, y, z, B_0) \rightarrow (-x, -y, -z, -B_0)$)

Date: March 13, 2014.

2010 Mathematics Subject Classification. 34D15, 34E13, 34E17, 34E20, 34C26, 37G15.

Key words and phrases. Bonhoeffer-van der Pol oscillator; Mixed-mode oscillations; Canards; Geometric singular perturbation theory; Blow-up technique.

The authors’ research was supported by the Research Foundation Flanders (FWO) under grant number G.0939.10N. Moreover, E. K. acknowledges support from the Polish Ministry of Science and Higher Education.

in Equation (1), allowing us to restrict our study to the regime where $B_0 > 0$ or, rather, to consider $B_0 \approx \frac{1}{2}$ only.) Mixed-mode oscillations (MMOs) are typically found in dynamical systems that evolve on multiple scales, and that are hence ‘fast-slow;’ see [3] and the references therein for details. Due to the oftentimes complex nature of these systems, the presence of MMOs is frequently established only numerically; almost equally often, it is proven by applying geometric singular perturbation theory [6, 10]. The latter approach crucially relies on a separation of scales to achieve a (partial) dimension reduction, thus allowing for a semi-analytical treatment in many cases. One downside of the geometric approach, however, is that, strictly speaking, it is only valid in the limit as $\varepsilon \rightarrow 0$, where ε defines the scale separation in the system. Fortunately, the analysis frequently does extend to ‘reasonable’ values of $\varepsilon > 0$; in fact, numerical evidence presented in Section 4 below suggests that the results obtained in this article may remain valid for ‘moderately large’ $\varepsilon (= 0.1)$.

Our aim here is to analyse Equation (1) from the point of view of geometric singular perturbation theory, focussing on a parameter regime that has not been considered in previous work [18, 7]: we will show that, for $0 \lesssim k_3 \ll 1$, Equation (1) evolves on three distinct time-scales, and we will describe in detail the corresponding mixed-mode dynamics, thus complementing the findings of Sekikawa *et al.* [18]. Specifically, it follows from (1c) that z is a ‘super-slow’ variable then; in fact, in the limit of $k_3 = 0$, z is constant, *i.e.*, the system reduces to a van der Pol-like oscillator that can undergo a ‘classical’ canard explosion [5, 14], transitioning from a stable equilibrium to relaxation oscillation via a family of canard cycles as z is varied. (Similarly, a reduction to a planar FitzHugh-Nagumo system is feasible when $k_3 = 1$: after introduction of $y + z$ as a new variable, it becomes apparent that the $(x, y + z)$ -equations decouple.) It is hence reasonable to assume that a canard phenomenon underlies the mixed-mode dynamics which is generated by Equation (1) when k_3 is non-zero, but small. In fact, the so-called ‘generalised canard mechanism’ [1] has been proposed as a unified generating mechanism for mixed-mode behaviour in singularly perturbed systems of equations such as (1): typically, MMOs are characterised by an alternation of small-amplitude oscillations (SAOs) that are followed by large excursions, or large-amplitude oscillations (LAOs). The former can frequently be shown to be due to (local) flow past a canard point, while the latter can be described by a (global) relaxation-like return mechanism. Periodic mixed-mode type orbits consisting of k SAOs and L LAOs are identified with the signature L^k ; knowledge of the possible signatures in a given system, in combination with estimates for the relevant parameter intervals, characterises completely the mixed-mode dynamics of the system.

In our case, with $0 \lesssim k_3 \ll 1$, such a characterisation is conveniently achieved by reducing Equation (1) to the simplified three time-scale model

$$(2a) \quad \varepsilon \dot{v} = -z + f_2 v^2 + f_3 v^3,$$

$$(2b) \quad \dot{z} = v - w,$$

$$(2c) \quad \dot{w} = \varepsilon(\mu - g_1 z),$$

which was proposed in [12] as representative for that type of system. Here, f_2 , f_3 , and g_1 denote fixed parameters, ε is assumed to be a small parameter, as above, and μ is the bifurcation parameter that unfolds the mixed-mode dynamics of (2).

While no comprehensive theory exists for perturbative scenarios that involve more than one singular parameter, in the seminal article [12], Krupa *et al.* characterised the mixed-mode dynamics that is generated by Equation (2). The authors then argued that their model is prototypical, in that it reflects the dynamical properties of three time-scale systems with similar local structure, as described in their article. While the analysis of [12] does not translate verbatim to the context of the extended Bonhoeffer-van der Pol oscillator, Equation (1), as we encounter additional terms in the reduced equations that are not present in (2), we nevertheless reach analogous conclusions on the resulting mixed-mode dynamics. Our study hence underpins the claim made in [12], namely,

that Equation (2) truly represents a canonical form. (We remark that a reduction of the so-called Wilson-Calloway model for the dopaminergic neuron [24] to (2) can be found in the related article [13]; our analysis will be similar in spirit to theirs.)

Finally, we note that the extended Bonhoeffer-van der Pol oscillator has been considered as a three time-scale system before, in [22], albeit in a slightly different formulation. Based on detailed asymptotics – which, incidentally, bears some resemblance to our approach – and numerical simulation, the author of that article was led to conclude the likely absence of stable periodic orbits of mixed-mode type in the system. Applying geometric singular perturbation theory, we disprove that conjecture rigorously.

This article is organised as follows. In Section 2, we study Equation (1) in the standard two time-scale form of geometric singular perturbation theory, with one fast variable x and two slow variables (y, z) . In Section 2.1, we describe the singular flow that is obtained for $\varepsilon = 0$ in (1). Then, in Section 2.2, we locate so-called ‘folded equilibria,’ which are crucial to the generation of canard-induced SAOs in the observed mixed-mode time series, and we identify a ‘folded saddle-node of type II’ (FSN II) [20, 15] as the ‘organising centre’ for the dynamics. In Section 2.3, we introduce a local formulation for Equation (1) close to that folded equilibrium; moreover, we define the bifurcation parameter μ – a combination of k_1 and B_0 – which unfolds the mixed-mode dynamics of (1). Finally, in Section 2.4, we apply standard geometric theory [6, 10] to approximate the global return mechanism which resets the flow to the SAO regime after passage through the fold region, and which hence accounts for the LAO portion of the resulting mixed-mode time series.

In Section 3, we perform a proper three-scale analysis of the transformed ‘localised’ version of (1) obtained in Section 2, under the additional assumption that $k_3 = \mathcal{O}(\varepsilon)$. (For simplicity, and in agreement with the parameter regime considered in [18], we will assume $k_3 = 0.1 = \varepsilon$.) In Section 3.1, we study the local dynamics near the folded saddle-node identified in Section 2.2 by means of a ‘blow-up’ transformation [5, 14] which uncovers the near-integrable structure of the equations, thus desingularising the flow there. Next, we describe the entry into, and the exit from, the fold region, which completes our analysis of the local dynamics. In Section 3.2, we then combine the resulting asymptotic estimates with our description of the global return, thus obtaining an approximation for the first-return map of the three time-scale Bonhoeffer-van der Pol oscillator. In Section 3.3, we discuss the bifurcation structure of that map, with a particular focus on secondary (‘bifurcating’) canards and sectors of rotation; then, in Section 3.4, we outline a reduction to an essentially one-dimensional map, which we analyse in accordance with [12, 13].

Finally, in Section 4, we discuss our findings, and we illustrate them numerically; moreover, we present potential pointers for future research.

2. TWO TIME-SCALE ANALYSIS

Assuming, for the time being, that the parameter k_3 in Equation (1c) does not scale with ε , we may interpret the equations in (1) as a fast-slow system in standard form that evolves on two distinct time-scales, the ratio of which is given by the singular perturbation parameter ε .

2.1. Reduced flow. Setting $\varepsilon = 0$ in (1) and considering the resulting reduced equations, we find the (two-dimensional) critical manifold

$$\mathcal{S}_0 := \{(x, y, z) \mid y = \varphi(x, z) = -x(1 - x^2) - z, (x, y, z) \in \mathcal{D} \subset \mathbb{R}^3\},$$

where $\mathcal{D} := [-x_0, x_0] \times [-y_0, y_0] \times [-z_0, z_0]$ is a compact subset of \mathbb{R}^3 with $z_0 > \frac{\sqrt{3}}{9}$, $y_0 > \frac{2\sqrt{3}}{9} + z_0$, and $x_0 > \frac{2\sqrt{3}}{3}$; the corresponding layer dynamics is given by horizontal fibres in the x -direction, with y and z fixed. Solving $\frac{\partial \varphi}{\partial x}(x, z) = -(1 - 3x^2) = 0$ for x , one then readily verifies that \mathcal{S}_0 is normally hyperbolic except at the two fold lines $\ell^\pm := \{(x, y, z) \mid x = \pm \frac{\sqrt{3}}{3}, y = -z \mp \frac{2\sqrt{3}}{9}, z \in [-z_0, z_0]\}$,

with z_0 as above. Hence, it follows that the manifold \mathcal{S}_0 can be written as the union of three sheets, $\mathcal{S}_0 = \mathcal{S}_0^{a-} \cup \mathcal{S}_0^r \cup \mathcal{S}_0^{a+}$, with $\mathcal{S}_0^{a\pm}$ attracting and \mathcal{S}_0^r repelling; here, \mathcal{S}_0^{a-} , \mathcal{S}_0^r , and \mathcal{S}_0^{a+} are defined by $x < -\frac{\sqrt{3}}{3}$, $x \in (-\frac{\sqrt{3}}{3}, \frac{\sqrt{3}}{3})$, and $x > \frac{\sqrt{3}}{3}$, respectively, with y and z varying accordingly. (An illustration of the resulting geometry – albeit in a transformed coordinate frame, to be introduced in Section 2.3 below – can be found in Figure 1; here, we remark that the assumptions on x_0 , y_0 , and z_0 in the definition of the set \mathcal{D} above are made precisely to encapsulate that geometry.) For $\varepsilon > 0$ sufficiently small, we then denote the corresponding sheets of the slow manifold \mathcal{S}_ε by $\mathcal{S}_\varepsilon^{a-}$, $\mathcal{S}_\varepsilon^r$, and $\mathcal{S}_\varepsilon^{a+}$, respectively.

Next, we recall that we have opted to consider only the regime where $B_0 > 0$ in (1); then, it is easy to verify that the ‘left’ fold line ℓ^- is always of jump type in that regime, with a slow flow that is pointed in the direction of increasing y . As is well known, geometric singular perturbation theory [6, 10] can be combined with the desingularisation technique known as ‘blow-up’ [4, 14] to describe the flow near ℓ^- ; see also [21], where the resulting relaxation dynamics is studied from a geometric point of view.

The flow near the ‘right’ fold ℓ^+ , on the other hand, is more involved; in particular, we argue that the presence of a (singular) Hopf bifurcation [8] near ℓ^+ for $B_0 \approx \frac{1}{2}$ suggests the occurrence of complicated canard-type dynamics there, *i.e.*, the existence of solutions that cross from the attracting sheet $\mathcal{S}_\varepsilon^{a+}$ to the repelling sheet $\mathcal{S}_\varepsilon^r$, staying near the latter for extended periods of time before being repelled away. To describe the corresponding dynamics, we first verify the presence of ‘folded equilibria’ [20, 23] in (1), which are a necessary prerequisite for the existence of canard trajectories.

2.2. Folded equilibria. To determine the folded equilibria of Equation (1), we proceed as in [13, Section 2.4]: we set $\varepsilon = 0$ in (1a) and then differentiate the relation $\varphi(x, z) - y = 0$ with respect to time τ , obtaining $\dot{y} = \frac{\partial \varphi}{\partial x} \dot{x} + \frac{\partial \varphi}{\partial z} \dot{z} = -(1 - 3x^2)\dot{x} - \dot{z}$. Substituting for \dot{y} and \dot{z} from (1b) and (1c), respectively, we have

$$-(1 - 3x^2)\dot{x} = -x + k_1[x(1 - x^2) + z] + B_0 + k_3(-x - k_1z + B_0).$$

Appending Equation (1c) and desingularising the resulting system by multiplication of the right-hand sides with a factor of $\frac{\partial \varphi}{\partial x}$, we find the projection of the reduced flow on \mathcal{S}_0 onto the (x, z) -plane in a neighbourhood of ℓ^+ :

$$(3a) \quad \dot{x} = -x + k_1[x(1 - x^2) + z] + B_0 - k_3(x + k_1z - B_0),$$

$$(3b) \quad \dot{z} = k_3(x + k_1z - B_0)(1 - 3x^2).$$

Now, ‘folded equilibria’ of Equation (1) [13] correspond to equilibrium points (x_+, z_+) of (3) that satisfy $\frac{\partial \varphi}{\partial x}(x_+, z_+) = 0$, and that are hence located at

$$(4) \quad x_+ = \frac{\sqrt{3}}{3} \quad \text{and} \quad z_+ = \frac{3\sqrt{3}(1 - \sqrt{3}B_0)(1 + k_3) - 2\sqrt{3}k_1}{9k_1(1 - k_3)}.$$

(‘Regular’ equilibria of (3), *i.e.*, equilibria that do not lie on ℓ^+ , are found by requiring that $x + k_1z - B_0 = 0$ and $-x + k_1[x(1 - x^2) + z] + B_0 = 0$ hold simultaneously.) For future reference, we note that z_+ depends on the parameters k_1 , k_3 , and – most importantly – B_0 . Since, moreover, $\frac{\partial \varphi}{\partial x} < 0$ for $-\frac{\sqrt{3}}{3} < x < \frac{\sqrt{3}}{3}$, the desingularisation leading to (3) effectively reverses the direction of the flow on \mathcal{S}_0^r , allowing for the existence of canard trajectories that can pass from \mathcal{S}_0^{a+} to \mathcal{S}_0^r via the folded equilibrium at $P^+ = (x_+, z_+)$; see again [20, 23] for details.

We claim that the point P^+ undergoes a saddle-node bifurcation on the fold line ℓ^+ for some critical value B_0^* of the parameter B_0 :

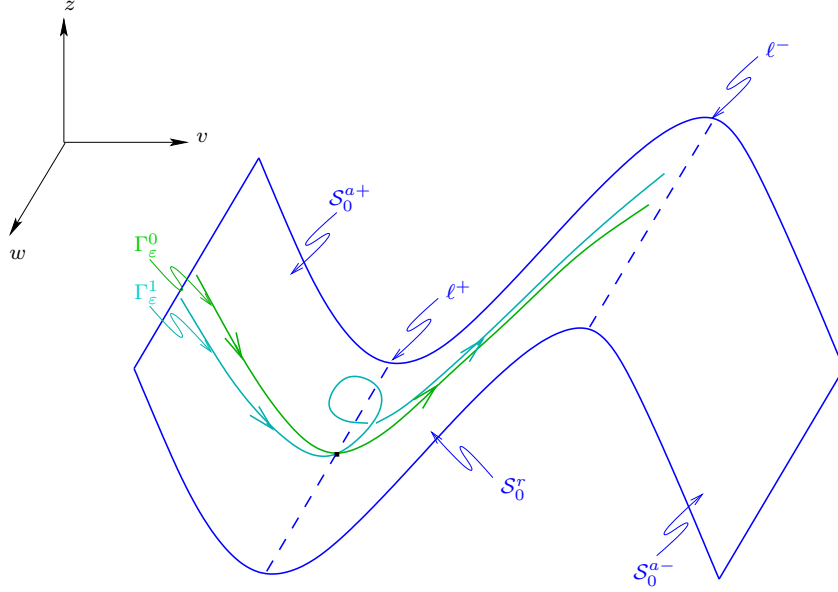


FIGURE 1. Geometry of Equation (6).

Lemma 1. *The folded equilibrium $P^+ = (x_+, z_+)$, with x_+ and z_+ defined as in Equation (4), undergoes a saddle-node bifurcation of type II as B_0 passes through $B_0^* \equiv \frac{\sqrt{3}}{9}(3 - k_1)$.*

Proof. Linearising Equation (3) about P^+ , we obtain

$$J = \begin{bmatrix} -(1 + k_3) & k_1(1 - k_3) \\ -4\sqrt{3}k_3 \frac{3\sqrt{3} - \sqrt{3}k_1 - 9B_0}{9(1 - k_3)} & 0 \end{bmatrix}$$

for the Jacobian of the reduced flow at (x_+, z_+) , as given in (4). Since the trace of J is $-(1 + k_3)$, while the determinant is of the order k_3 , we deduce that one of the eigenvalues of J equals $-1 + \mathcal{O}(k_3)$, while the other is $\mathcal{O}(k_3)$. Solving $\det J = 0$ for B_0 , we find that the latter eigenvalue equals zero for $3 - k_1 - 3\sqrt{3}B_0 = 0$, which yields $B_0 = \frac{\sqrt{3}}{9}(3 - k_1) \equiv B_0^*$, as claimed.

Finally, it is straightforward to verify that the eigendirection corresponding to the zero eigenvalue for $B_0 = B_0^*$ is transverse to the fold line ℓ^+ , *i.e.*, that P^+ is a *folded saddle-node of type II*; see [20] for details. (In fact, one calculates that the eigenvalue-eigenvector pairs of J for $B_0 = B_0^*$ are given by $\{-(1 + k_3), (1, 0)\}$ and $\{0, (k_1 \frac{1 - k_3}{1 + k_3}, 1)\}$, respectively.) \square

Remark 1. Alternatively, one can determine B_0^* by considering the $(2, 1)$ -entry of the Jacobian J : B_0^* is precisely the value of B_0 for which that entry equals zero. \square

In sum, one hence obtains the following picture for the projected reduced flow of Equation (1): when $B_0 > B_0^*$, a stable node equilibrium exists on the ‘right’ (attracting) sheet \mathcal{S}_0^{a+} of \mathcal{S}_0 , while P^+ is a folded saddle; for $B_0 = B_0^*$, that equilibrium coalesces with P^+ in a transcritical bifurcation of a saddle and a node, *i.e.*, the point P^+ undergoes a saddle-node bifurcation on the fold ℓ^+ . (In fact, one can show that P^+ is both a regular and a folded equilibrium in that case.) Finally, when $B_0 < B_0^*$ – which is the regime we are interested in – P^+ is a folded node, while a saddle equilibrium is found on the ‘middle’ (repelling) sheet \mathcal{S}_0^r of \mathcal{S}_0 .

2.3. Local formulation. In this subsection, we rewrite Equation (1) in a form that is more suitable for the following analysis; to that end, we perform a series of coordinate changes which transform

(1) into an equivalent set of equations that is centred on the ‘right’ fold line ℓ^+ . We begin by translating the folded equilibrium at P^+ to the origin by introducing the new variables

$$v = -(x - x_+), \quad p = y + z - (y_+ + z_+) = y + z + \frac{2}{9}\sqrt{3}, \quad \text{and} \quad q = z - z_+;$$

here, x_+ and z_+ are defined as in Equation (4), while the constant in the definition of p is obtained by solving $0 = x_+(1 - x_+^2) + y_+ + z_+$, as found from (1a), for $y_+ + z_+$. (The change of sign in the definition of v additionally reflects the critical manifold \mathcal{S}_0 about the q -axis, thus bringing it into a more familiar configuration; clearly, that reflection reverses the location of the two sheets $\mathcal{S}_\varepsilon^{a\pm}$, with $\mathcal{S}_\varepsilon^{a+}$ becoming the ‘left’ attracting sheet and $\mathcal{S}_\varepsilon^{a-}$ the ‘right’ one.)

The system of equations resulting from the above transformation is given by

$$\begin{aligned} (5a) \quad & \varepsilon \dot{v} = \sqrt{3}v^2 - v^3 - p, \\ (5b) \quad & \dot{p} = (1 + k_3)v + k_1(1 - k_3)q - k_1p, \\ (5c) \quad & \dot{q} = k_3(v - k_1q - \mu), \end{aligned}$$

where $\mu = \frac{2}{1-k_3}(B_0^* - B_0)$ denotes a new parameter, with B_0^* defined as in the statement of Lemma 1.

Finally, to reduce these equations to a form that is as close as possible to the canonical system in (2), we rescale q by introducing the new variable $w = -k_1q$, and we abuse notation slightly, relabelling p as z for consistency with [12]:

$$\begin{aligned} (6a) \quad & \varepsilon \dot{v} = \sqrt{3}v^2 - v^3 - z, \\ (6b) \quad & \dot{z} = (1 + k_3)v - (1 - k_3)w - k_1z, \\ (6c) \quad & \dot{w} = k_1k_3(\mu - w - v). \end{aligned}$$

For future reference, we remark that the critical manifold \mathcal{S}_0 is given by $z = f(v) := \sqrt{3}v^2 - v^3$ in the context of Equation (6); the corresponding reduced geometry of (1) in the singular limit of $\varepsilon = 0$ is sketched in Figure 1.

2.4. Global return mechanism. Before considering in detail the local dynamics of (6) in a neighbourhood of the fold line ℓ^+ , we discuss the global return mechanism which reinjects the flow into the fold region after relaxation has occurred. As in [12, Section 2.1], we first define two sections, a section $\Sigma^{\text{in}} : \{v = -\rho\}$ through the attracting sheet \mathcal{S}_0^{a+} and a section $\Sigma^{\text{out}} : \{v = \delta\}$ across the fast foliation of \mathcal{S}_0 , with $\rho, \delta > 0$ small, but fixed, and $|z|$ and $|w|$ bounded; see Figure 2 for an illustration. The global return from Σ^{out} to Σ^{in} under the flow of (6) can then be approximated to leading order via the slow evolution of v along the attracting sheets \mathcal{S}_0^{a-} and \mathcal{S}_0^{a+} of the critical manifold \mathcal{S}_0 , as illustrated in Figure 3; in particular, one may neglect the transition from ℓ^+ to \mathcal{S}_0^{a-} and from ℓ^- to \mathcal{S}_0^{a+} , respectively, under the corresponding layer flow, as was also done in [12, Section 2.5].

Thus, we have the following result on the leading-order asymptotics of the map $\Pi^{\text{ret}} : \Sigma^{\text{out}} \rightarrow \Sigma^{\text{in}}$, the proof of which closely follows [12, Section 2.5] and [13, Section 3.3]:

Lemma 2. *Let $w_0 > 0$ be sufficiently small; then, the w -component of the global return map $\Pi^{\text{ret}} : \Sigma^{\text{out}} \rightarrow \Sigma^{\text{in}}$ satisfies*

$$(7) \quad \hat{w} := \Pi^{\text{ret}}(w) = w + k_1k_3 \left[3 \left(1 - \frac{1}{2}k_1 \right) \mu - \frac{1}{2}\sqrt{3}k_1 \right]$$

to leading order in k_3 and ε , for any $w \in [-w_0, w_0] \subset \Sigma^{\text{out}}$.

Proof. We consider the projection of the reduced flow corresponding to Equation (6) onto the critical manifold \mathcal{S}_0 , the accuracy of which will be sufficient for deriving the leading-order approximation for Π^{ret} considered here; cf. also [12, Section 2.5]. Proceeding as in Section 2.2, *i.e.*, noting that

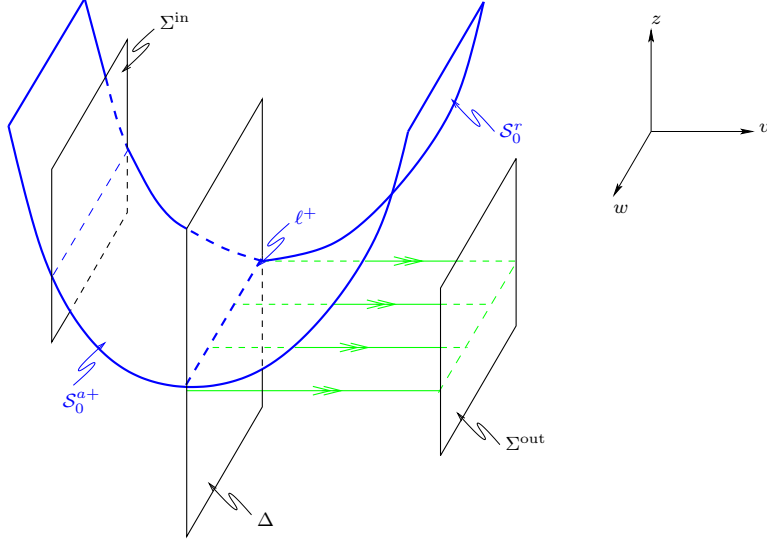


FIGURE 2. Sections for the flow of (6).

$z = f(v)$ implies $\dot{z} = f'(v)\dot{v}$ and desingularising the resulting (v, w) -system by multiplication with a factor of $-f'(v)$, which is positive on the two attracting sheets \mathcal{S}_0^{\pm} of \mathcal{S}_0 , we find

$$(8a) \quad \dot{v} = -(1 + k_3)v + (1 - k_3)w + k_1 f(v),$$

$$(8b) \quad \dot{w} = -k_1 k_3 f'(v)(\mu - v - w).$$

Next, we note that $w = \mathcal{O}(1)$ in the parameter regime which is of interest to us, as $0 \lesssim k_3 \ll 1$ then, whereas $v = \mathcal{O}(1)$ and $z = \mathcal{O}(1)$ during the global return phase. (Specifically, numerical evidence suggests that one may assume $w = \mathcal{O}(k_3)$ throughout; see also Assumption 1 below.) Hence, approximating (8a) by $\dot{v} \approx -v + k_1 f(v)$ and neglecting the w -dependence in (8b), we obtain

$$(9) \quad \frac{dw}{dv} = k_1 k_3 \frac{f'(v)(\mu - v)}{v - k_1 f(v)},$$

to lowest order in k_3 and ε . Now, we observe that, with k_1 fixed, the condition $|k_1 \frac{f(v)}{v}| < 1$ is certainly satisfied for v in some appropriately chosen (compact) interval. (In fact, for $k_1 = 0.35$, as in [18], it suffices to take $v \in [v_{\max}^*, v_0]$, where v_{\max}^* and v_0 are defined below, as $|\frac{f(v)}{v}| \leq \frac{4}{3}$ on that interval.) Hence, we may approximate $\frac{1}{v - k_1 f(v)} \approx \frac{1}{v} [1 + k_1 \frac{f(v)}{v}]$, which implies

$$(10) \quad \frac{dw}{dv} = k_1 k_3 \frac{f'(v)}{v} (\mu - v) \left[1 + k_1 \frac{f(v)}{v} \right].$$

Finally, following [12, 13], we define

$$\mathcal{G}(v^*, v, \mu) := k_1 \int_{v^*}^v \frac{f'(\sigma)}{\sigma} (\mu - \sigma) \left[1 + k_1 \frac{f(\sigma)}{\sigma} \right] d\sigma;$$

then, we may write the leading-order solution to (10) as $\hat{w} = w + k_3 [\mathcal{G}(v_0, v_{\max}, \mu) + \mathcal{G}(v_{\max}^*, -\rho, \mu)]$, where the limits of integration are defined as $v_{\max} = \frac{2}{3}\sqrt{3}$, $v_{\max}^* = -\frac{1}{3}\sqrt{3}$, and $v_0 = \sqrt{3}$, with ρ as in the definition of the section Σ^{in} above. (Here, we have adopted the notation of [12], where v_{\max} is the value of v for which f attains its local maximum, $v_{\max}^* < 0$ is defined by the requirement that $f(v_{\max}^*) = f(v_{\max})$, and $v_0 > 0$ is the second, non-trivial zero of f ; cf. again Figure 3.) Replacing $\mathcal{G}(v_{\max}^*, -\rho, \mu)$ with $\mathcal{G}(v_{\max}^*, 0, \mu)$, as was done in [12, Section 2.5], and evaluating the resulting integrals, we find (7), as claimed, which completes the proof. \square

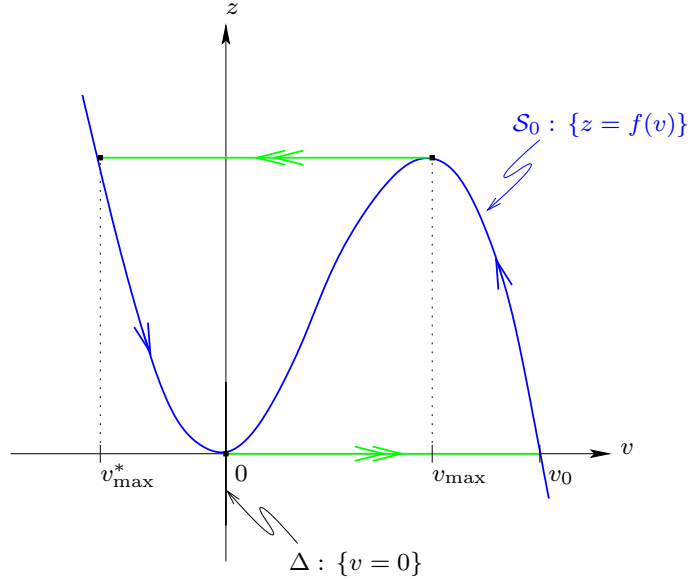


FIGURE 3. Geometry of global return.

Remark 2. While Π^{ret} is a function of the two variables z and w , it reduces to a one-dimensional map (in w) to the order considered here, by Equation (7). Hence, we have opted to suppress the z -dependence of Π^{ret} in our notation. \square

In particular, given Lemma 2, we may approximate the critical value μ^c of μ beyond which the flow of (6) exhibits pure relaxation oscillation: requiring that $\hat{w} = w$ in (7), as in [12, Section 2.5], *i.e.*, solving the term in square brackets therein for μ , we have

Corollary 1. *The critical μ -value μ^c for which mixed-mode dynamics ceases to exist in Equation (6) is given by $\mu^c = \frac{1}{3} \frac{\sqrt{3}k_1}{2-k_1}$, to lowest order in k_3 and ε .*

Evaluating μ for $k_1 = 0.35$, as in [18], we obtain $\mu^c = 0.070\sqrt{3} \approx 0.12247$, which is in good agreement with numerical simulation; see Section 4 below. (In fact, explicit integration of (9), and evaluation at the same limits as in the proof of Lemma 2, yields $\mu^c \approx 0.09769$, which is well within $\mathcal{O}(k_3^2, k_3\varepsilon)$ of the estimate given in Corollary 1, as expected.)

Remark 3. For future reference, we note that Equation (7) yields an approximation for Π^{ret} which is accurate up to an $\mathcal{O}(\varepsilon^2 \ln \varepsilon)$ -error when $k_3 = \varepsilon$, as is assumed in the following section. In fact, projecting the flow of (6) onto the slow manifold \mathcal{S}_ε instead of onto \mathcal{S}_0 , one can show that the error incurred by Equations (8) and (9) is of the order $\mathcal{O}(\varepsilon^2)$ when $w = \mathcal{O}(\varepsilon)$, while an $\mathcal{O}(\varepsilon^2 \ln \varepsilon)$ -contribution is introduced through passage past the fold line ℓ^- ; see [21, Theorem 1] for details. \square

3. THREE TIME-SCALE ANALYSIS

Given the parameter regime studied by Sekikawa *et al.* [18], with $k_1 = 0.35$ and $\varepsilon = 0.1$, it seems reasonable to set $k_3 = \varepsilon$ in Equation (6); then, the variable w will vary on a third (‘super-slow’) time scale, as (6c) implies $\dot{w} = \mathcal{O}(\varepsilon)$ throughout. (Since, clearly, $v = \mathcal{O}(1)$ and $z = \mathcal{O}(1)$ during relaxation, cf. the proof of Lemma 2 as well as Figure 3, it follows that the variables v and z will remain ‘fast’ and ‘slow,’ respectively.) Hence, replacing k_3 with ε and writing κ instead of k_1 for

compactness, we obtain the system of equations

$$(11a) \quad \varepsilon \dot{v} = \sqrt{3}v^2 - v^3 - z,$$

$$(11b) \quad \dot{z} = v - w - \kappa z + \varepsilon(v + w),$$

$$(11c) \quad \dot{w} = \varepsilon \kappa(\mu - w - v)$$

from (6) which, together with the corresponding fast system

$$(12a) \quad v' = \sqrt{3}v^2 - v^3 - z,$$

$$(12b) \quad z' = \varepsilon[v - w - \kappa z + \varepsilon(v + w)],$$

$$(12c) \quad w' = \varepsilon^2 \kappa(\mu - w - v),$$

will be the starting point for our study of the three time-scale Bonhoeffer-van der Pol oscillator. (Here, the prime denotes differentiation with respect to the fast time $t = \frac{\tau}{\varepsilon}$.)

In the remainder of this article, we will characterise the mixed-mode dynamics that is induced by the flow of Equation (11); as we will show below, the resulting asymptotics will be very similar ‘qualitatively’ to the picture painted in [12], even if some of the specifics of the analysis will differ. Following [12, 13], we will restrict the parameter μ – which we have identified as the relevant bifurcation parameter above – to some interval $(\underline{\mu}, \bar{\mu})$ on which stable ‘mixed’ MMO dynamics can unfold in (11). Since we will not consider the ‘pure’ relaxation (LAO) regime in (11), where $\mu > \mu^c$, we must have $\bar{\mu} \lesssim \mu^c$. However, we will also disregard the purely oscillatory (SAO) regime that is obtained for μ close to zero: as numerical simulation implies the occurrence of a (singular) Hopf bifurcation [8] $\mathcal{O}(\varepsilon)$ -close to the fold at ℓ^+ – and, hence, the onset of small-amplitude oscillatory dynamics – for $\mu \equiv \mu^H \approx 0.02072$, it follows that $\underline{\mu} \gtrsim \mu^H$ must hold; see Section 4 below for details.

It remains to show that the interval $(\underline{\mu}, \bar{\mu})$ is non-empty: since $\mu^c = \mathcal{O}(\varepsilon)$ in the parameter regime considered here, as stated in Section 2.4 above, while $\mu^H = \mathcal{O}(\varepsilon^2)$, we may conclude that the width of $(\underline{\mu}, \bar{\mu})$ is of the order $\mathcal{O}(\varepsilon^\alpha)$ for some $1 < \alpha < 2$ and, hence, that non-trivial mixed-mode dynamics will be observed in (11) as μ is varied in that interval; cf. also the discussion towards the end of [12, Section 2.2].

3.1. Local dynamics. In this subsection, we consider Equation (11) locally, in a neighbourhood of ℓ^+ . To that end, we first analyse the dynamics of (11) – or, equivalently, of (12) – in the fold region itself, by introducing an appropriate rescaling of the variables (v, z, w) near ℓ^+ ; then, we study the mechanisms which govern the entry of the flow into that region and the exit from it, respectively.

3.1.1. Fold region. To describe the dynamics of Equation (12) in a neighbourhood of the fold line ℓ^+ , we rescale the vector field there by writing

$$(13) \quad v = \sqrt{\varepsilon} \bar{v}, \quad z = \varepsilon \bar{z}, \quad w = \sqrt{\varepsilon} \bar{w}, \quad \text{and} \quad \bar{t} = \sqrt{\varepsilon} t.$$

Substituting into (12) and simplifying, we obtain the desingularised system of equations

$$(14a) \quad \bar{v}' = \sqrt{3}\bar{v}^2 - \bar{z} - \sqrt{\varepsilon}\bar{v}^3,$$

$$(14b) \quad \bar{z}' = \bar{v} - \bar{w} - \kappa\sqrt{\varepsilon}\bar{z} + \varepsilon(\bar{v} + \bar{w}),$$

$$(14c) \quad \bar{w}' = \varepsilon\kappa[\mu - \sqrt{\varepsilon}(\bar{w} + \bar{v})];$$

as pointed out in [12], in the context of Equation (2), the scale separation between v and z has been eliminated by the rescaling in (13). (Here, the prime now denotes differentiation with respect to the new time \bar{t} ; however, for simplicity of notation, we will frequently omit the bar in the following, writing again t instead.)

Based on numerical evidence (data not shown), we expect that $w = \mathcal{O}(\varepsilon)$ in Equation (12), uniformly in t ; see also the proof of Lemma 2 above. Correspondingly, we will henceforth make

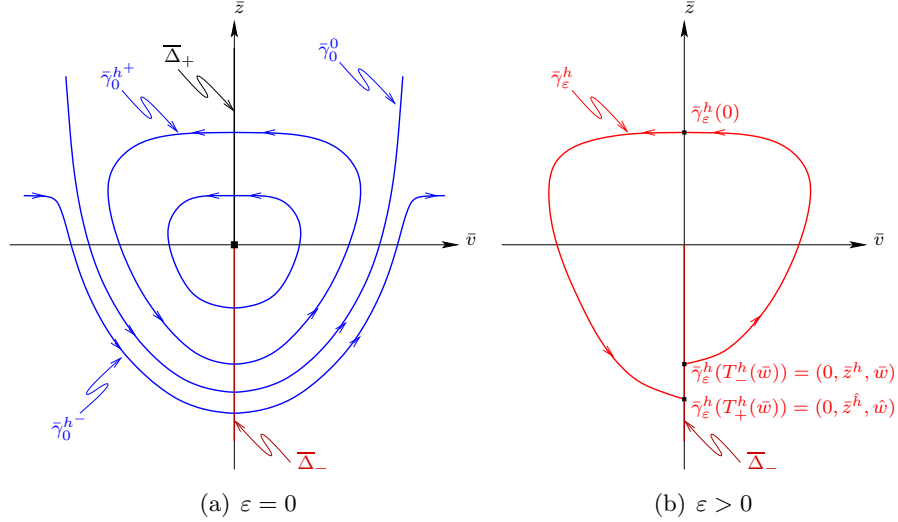


FIGURE 4. Dynamics of Equation (14).

the following assumption on $\bar{w} = \frac{w}{\sqrt{\varepsilon}}$, which may be verified *a posteriori* for the parameter regime considered here; details can be found in [12, Section 2.2].

Assumption 1. Let $\varepsilon \in [0, \varepsilon_0]$, with $\varepsilon_0 > 0$ sufficiently small; then, $\bar{w} = \mathcal{O}(\sqrt{\varepsilon})$ as $\varepsilon \rightarrow 0^+$ in (14), uniformly in \bar{t} .

In the singular limit, *i.e.*, for $\varepsilon = 0$, Equation (14) reduces to the planar system

$$(15) \quad \begin{aligned} \bar{v}' &= \sqrt{3}\bar{v}^2 - \bar{z}, \\ \bar{z}' &= \bar{v} - \bar{w}, \end{aligned}$$

in which \bar{w} is a (constant) parameter. The resulting flow is well-understood, as it underlies the study of classical two-dimensional canard explosion [5, 14]. In particular, Equation (15) is integrable for $\bar{w} = 0$, with a constant of motion of the form

$$(16) \quad H(\bar{v}, \bar{z}) = \frac{1}{2}e^{-2\sqrt{3}\bar{z}} \left(-\bar{v}^2 + \frac{\sqrt{3}}{3}\bar{z} + \frac{1}{6} \right);$$

see also [12, Equation (2.5)]. Thus, level curves for (15) are defined by $H(\bar{v}, \bar{z}) = h$, with h real; the singular solution corresponding to $h = 0$, which is given by

$$(17) \quad \bar{\gamma}_0^0(t) = (\bar{v}_0^0, \bar{z}_0^0)(t) = \left(\frac{\sqrt{3}}{6}t, \frac{\sqrt{3}}{12}t^2 - \frac{\sqrt{3}}{6} \right),$$

cf. [12, Equation (2.6)], separates the closed level curves of H that are obtained for $h > 0$ from the open ones, which are characterised by $h < 0$. (Clearly, the former yield periodic solutions to Equation (15), while the latter correspond to trajectories that leave the fold region; see [12] for details.) The geometry of (14) in the singular limit is illustrated in Figure 4(a).

As in [12, Section 2.2], we introduce the following notation: we write $\bar{\Delta}$ for the plane $v = 0$, with (z, w) in some compact subset of \mathbb{R}^2 ; see again Figure 2. Then, $\bar{\Delta}_+$ denotes that same plane in the rescaled coordinates defined in (13), while $\bar{\Delta}_-$ stands for the half-plane $\bar{\Delta} \cap \{\bar{z} < 0\}$.

Remark 4. Here and in the following, \square will denote any object in the original (v, z, w) -coordinates, while the equivalent ‘blown-up’ object in $(\bar{v}, \bar{z}, \bar{w})$ -space will be written as $\bar{\square}$. \square

In our analysis, we will sometimes parametrise trajectories of (15) by their unique h -value; thus, we will write \bar{z}^h for the corresponding (unique) value of \bar{z} in $\bar{\Delta}_-$. Moreover, denoting by $\bar{\gamma}_\varepsilon^h(t)$ the solution to (14) which contains the point $(0, \bar{z}^h, \bar{w})$, we will assume that the time parametrisation is such that $\bar{\gamma}_\varepsilon^h(0)$ lies in $\bar{\Delta}_+ = \bar{\Delta} \setminus \bar{\Delta}_-$, as shown in Figure 4(b). Let $T_\pm^h(\bar{w})$ denote the times for which $\bar{\gamma}_\varepsilon^h(T_\pm^h(\bar{w})) \in \bar{\Delta}_-$, where we note that, clearly, $T_-^h(\bar{w}) < 0 < T_+^h(\bar{w})$; see again Figure 4(b). Then, we write $T^h(\bar{w}) := T_+^h(\bar{w}) - T_-^h(\bar{w})$ for the return time to $\bar{\Delta}_-$ under the flow of Equation (14); for brevity, we define $T^h := T_+^h(0)$. Finally, one can show as in [12, Lemma A.2] that

$$(18) \quad T^h = \sqrt{-2 \ln h} + \mathcal{O}(1);$$

the above estimate will prove useful, since it implies $T^h = \mathcal{O}(\sqrt{-\ln \varepsilon})$ whenever $h = \mathcal{O}(\varepsilon^M)$ for some $M > 0$, as will be the case throughout the remainder of this section.

An approximation for the transition map $\bar{\Pi} : \bar{\Delta}_- \rightarrow \bar{\Delta}_-$, which describes the dynamics of (14) in the small-amplitude regime, can then be obtained in analogy to [12, Proposition 2.2]; we merely outline the derivation here, focussing on points at which the corresponding proof requires modification:

Proposition 1. *Let $\varepsilon \in [0, \varepsilon_0]$, with $\varepsilon_0 > 0$ sufficiently small, and suppose that $h = \mathcal{O}(\varepsilon^M)$ for some $M > 0$. Then, the transition map $\bar{\Pi} : \bar{\Delta}_- \rightarrow \bar{\Delta}_-$ for (14) is of the form*

$$(19) \quad (\hat{h}, \hat{w}) := \bar{\Pi}(h, \bar{w}) = (h + \sqrt{\varepsilon} d_{\sqrt{\varepsilon}}^h + \bar{w} d_{\bar{w}}^h + \mathcal{O}[(\sqrt{\varepsilon} + \bar{w})^2], \bar{w} + \varepsilon \kappa \mu T^h(\bar{w}) + \mathcal{O}(\varepsilon \sqrt{\varepsilon})),$$

where

$$(20) \quad d_{\sqrt{\varepsilon}}^h = \int_{-T^h}^{T^h} \nabla H(\bar{\gamma}_0^h(t)) \cdot (-\bar{v}_0^h(t)^3, -\kappa \bar{z}_0^h(t))^T dt$$

and

$$(21) \quad d_{\bar{w}}^h = \int_{-T^h}^{T^h} \nabla H(\bar{\gamma}_0^h(t)) \cdot (0, -1)^T dt.$$

Proof. The expression for the h -component of $\bar{\Pi}$ is obtained via an adaptation of the argument in [12, Section 2.2]: due to the presence of an additional term of the order $\mathcal{O}(\sqrt{\varepsilon} \bar{z})$, Equation (14b) is not in the form of the extended system formulated in [12, Equation (2.8)]. However, denoting by \hat{h} the image of h under $\bar{\Pi}$, we still have

$$\begin{aligned} \hat{h} - h &= H(0, \bar{z}^{\hat{h}}) - H(0, \bar{z}^h) = \int_{T_-^h(\bar{w})}^{T_+^h(\bar{w})} \frac{d}{dt} H(\bar{\gamma}_\varepsilon^h(t)) dt \\ &\sim \int_{T_-^h(\bar{w})}^{T_+^h(\bar{w})} \nabla H(\bar{\gamma}_0^h(t)) \cdot (\bar{v}', \bar{z}')^T \Big|_{\bar{\gamma}_0^h(t)} dt = \sqrt{\varepsilon} d_{\sqrt{\varepsilon}}^h + \bar{w} d_{\bar{w}}^h; \end{aligned}$$

thus, the only difference to the proof of [12, Proposition 2.2] lies in the definition of the coefficient $d_{\sqrt{\varepsilon}}^h$ in (20), as was also the case in the corresponding Equation (45a) of [13]. (In fact, a straightforward calculation shows that the contribution from the \bar{z} -dependent term in (14b) to that coefficient is non-zero.)

Similarly, the derivation of the \bar{w} -component of $\bar{\Pi}$ has to be adapted slightly, as we cannot simply integrate Equation (14c). Instead, we express \bar{v} from (14b) and substitute into (14c), obtaining

$$(22) \quad \bar{w}' = -2\kappa \varepsilon \sqrt{\varepsilon} \bar{w} + \varepsilon \kappa [\mu - \sqrt{\varepsilon} \bar{z}'(t)] + \mathcal{O}(\varepsilon^2).$$

The solution of the corresponding homogeneous equation is given by $\bar{w}_h = C e^{-2\kappa\varepsilon\sqrt{\varepsilon}t}$. By variation of constants, we find $C'(t) = \varepsilon\kappa(\mu - \sqrt{\varepsilon}\bar{z}')e^{2\kappa\varepsilon\sqrt{\varepsilon}t}$ and, hence,

$$C(t) = \frac{\mu}{2\sqrt{\varepsilon}}(e^{2\kappa\varepsilon\sqrt{\varepsilon}t} - e^{2\kappa\varepsilon\sqrt{\varepsilon}T_-^h(\bar{w})}) - \kappa\varepsilon\sqrt{\varepsilon} \int_{T_-^h(\bar{w})}^t \bar{z}'(s)e^{2\kappa\varepsilon\sqrt{\varepsilon}s} ds$$

after integration. (Here, $T_-^h(\bar{w})$ is defined as above; in particular, we cannot simply translate the initial time to zero, as Equation (22) is non-autonomous.) The full solution to (22) can then be expressed as

$$(23) \quad \bar{w}(t) = C e^{-2\kappa\varepsilon\sqrt{\varepsilon}t} + \frac{\mu}{2\sqrt{\varepsilon}}(1 - e^{-2\kappa\varepsilon\sqrt{\varepsilon}[t - T_-^h(\bar{w})]}) - \kappa\varepsilon\sqrt{\varepsilon} \int_{T_-^h(\bar{w})}^t \bar{z}'(s)e^{2\kappa\varepsilon\sqrt{\varepsilon}s} ds \cdot e^{-2\kappa\varepsilon\sqrt{\varepsilon}t}.$$

Writing \bar{w} for the initial value of $\bar{w}(t)$ to determine $C = \bar{w}e^{2\kappa\varepsilon\sqrt{\varepsilon}T_-^h(\bar{w})}$ in (23), evaluating the resulting expression at $T_+^h(\bar{w})$ – *i.e.*, after the return to $\bar{\Delta}_-$ has been completed – and expanding the exponential term via $e^{-2\kappa\varepsilon\sqrt{\varepsilon}t} = 1 - 2\kappa\varepsilon\sqrt{\varepsilon}t + \mathcal{O}(\varepsilon^3 t^2)$, we find

$$(24) \quad \hat{w} = \bar{w}[1 - 2\kappa\varepsilon\sqrt{\varepsilon}T^h(\bar{w})] + \varepsilon\kappa\mu T^h(\bar{w}) - \kappa\varepsilon\sqrt{\varepsilon} \int_{T_-^h(\bar{w})}^{T_+^h(\bar{w})} \bar{z}'(t)e^{2\kappa\varepsilon\sqrt{\varepsilon}t} dt \cdot e^{-2\kappa\varepsilon\sqrt{\varepsilon}T_+^h(\bar{w})} + \mathcal{O}(\varepsilon^2).$$

(Here, we recall that $T^h(\bar{w}) = T_+^h(\bar{w}) - T_-^h(\bar{w})$ denotes the return time to $\bar{\Delta}_-$, as before.) Since $\bar{w} = \mathcal{O}(\sqrt{\varepsilon})$, and since we may assume $T^h(\bar{w}) = \mathcal{O}(\sqrt{-\ln \varepsilon})$, see also Equation (18), we can neglect the $2\kappa\varepsilon\sqrt{\varepsilon}\bar{w}T^h(\bar{w})$ -term in (24). Hence, it remains to estimate the integral term therein: integrating by parts, we obtain

$$\begin{aligned} & \int_{T_-^h(\bar{w})}^{T_+^h(\bar{w})} \bar{z}'(t)e^{2\kappa\varepsilon\sqrt{\varepsilon}t} dt \cdot e^{-2\kappa\varepsilon\sqrt{\varepsilon}T_+^h(\bar{w})} \\ &= \bar{z}(t)e^{2\kappa\varepsilon\sqrt{\varepsilon}t} \Big|_{T_-^h(\bar{w})}^{T_+^h(\bar{w})} \cdot e^{-2\kappa\varepsilon\sqrt{\varepsilon}T_+^h(\bar{w})} - 2\kappa\varepsilon\sqrt{\varepsilon} \int_{T_-^h(\bar{w})}^{T_+^h(\bar{w})} \bar{z}(t)e^{2\kappa\varepsilon\sqrt{\varepsilon}t} dt \cdot e^{-2\kappa\varepsilon\sqrt{\varepsilon}T_+^h(\bar{w})}. \end{aligned}$$

Now, taking into account that $\bar{z} = \mathcal{O}(1)$ in the fold region, as well as that the exponential factor multiplying the second (integral) term on the right-hand side is bounded by one, the contribution from the latter is clearly of higher order; the first (boundary) term gives

$$\begin{aligned} \bar{z}(t)e^{2\kappa\varepsilon\sqrt{\varepsilon}t} \Big|_{T_-^h(\bar{w})}^{T_+^h(\bar{w})} \cdot e^{-2\kappa\varepsilon\sqrt{\varepsilon}T_+^h(\bar{w})} &= \left[\bar{z}(T_+^h(\bar{w}))e^{2\kappa\varepsilon\sqrt{\varepsilon}T_+^h(\bar{w})} - \bar{z}(T_-^h(\bar{w}))e^{2\kappa\varepsilon\sqrt{\varepsilon}T_-^h(\bar{w})} \right] e^{-2\kappa\varepsilon\sqrt{\varepsilon}T_+^h(\bar{w})} \\ &= \bar{z}(T_+^h(\bar{w})) - \bar{z}(T_-^h(\bar{w})) + \mathcal{O}(\varepsilon\sqrt{\varepsilon}T_{\pm}^h(\bar{w})) \end{aligned}$$

to leading order, since any exponential factors that occur can again be approximated by $1 + \mathcal{O}(\varepsilon\sqrt{\varepsilon}T_{\pm}^h(\bar{w}))$, and since $\bar{z}(T_{\pm}^h(\bar{w})) = \mathcal{O}(1)$. Finally, we claim that $\bar{z}(T_+^h(\bar{w})) - \bar{z}(T_-^h(\bar{w})) = \mathcal{O}(\sqrt{\varepsilon})$, which is easily verified by considering the constant of motion H , as defined in Equation (16): assuming that $H(0, \bar{z}(T_+^h(\bar{w}))) - H(0, \bar{z}(T_-^h(\bar{w}))) = \mathcal{O}(\sqrt{\varepsilon})$ in $\bar{\Delta}_-$, one can solve perturbatively for $\bar{z}(T_+^h(\bar{w}))$ in terms of $\bar{z}(T_-^h(\bar{w}))$. (Alternatively, one may resort to the well-known asymptotics of the Lambert W function [17, Section 1.5].)

In sum, it follows that the integral term in (24) is of the order $\mathcal{O}(\varepsilon^2)$, which implies $\hat{w} = \bar{w} + \varepsilon\kappa\mu T^h(\bar{w}) + \mathcal{O}(\varepsilon\sqrt{\varepsilon})$, as claimed, completing the proof. \square

3.1.2. Entry mechanism. Next, we consider the entry of the flow induced by Equation (12) into the fold region; in other words, we will approximate the transition between the sections Σ^{in} and $\bar{\Delta}_-$, as defined in Sections 2.4 and 3.1.1, respectively. Following [12, Section 2.3], we introduce an ‘intermediate’ section $\bar{\Delta}^{\text{in}}$: $\{\bar{v} = -\alpha\}$ (in rescaled coordinates), with $0 < \alpha < \rho$ small and fixed.

Correspondingly, in the proof of Proposition 2 below, we first study the transition between Σ^{in} and Δ^{in} , followed by that between $\bar{\Delta}^{\text{in}}$ and $\bar{\Delta}_-$:

Proposition 2. *Let $(z^{\text{in}}, w^{\text{in}}) \in \Sigma^{\text{in}}$; then, for $\varepsilon \in [0, \varepsilon_0]$ sufficiently small, the transition map $\Pi^{\text{in}} : \Sigma^{\text{in}} \rightarrow \bar{\Delta}_-$ satisfies*

$$(25) \quad (h^-, \bar{w}^-) := \Pi^{\text{in}}(z^{\text{in}}, w^{\text{in}}) \\ = \left(\sqrt{\varepsilon} d_{\sqrt{\varepsilon}}^- + \frac{w^{\text{in}}}{\sqrt{\varepsilon}} d_{\bar{w}}^- + \mathcal{O}[(\sqrt{\varepsilon} + \bar{w})^2], \frac{w^{\text{in}}}{\sqrt{\varepsilon}} + w^{\text{in}} \sqrt{3} \kappa \mu \sqrt{\varepsilon} \ln \varepsilon + \mathcal{O}(\sqrt{\varepsilon}) \right),$$

where

$$d_{\sqrt{\varepsilon}}^- = \int_{-\infty}^0 \nabla H(\bar{\gamma}_0^0(t)) \cdot (-\bar{v}_0^0(t)^3, -\kappa \bar{z}_0^0(t))^T dt \quad \text{and} \quad d_{\bar{w}}^- = \int_{-\infty}^0 \nabla H(\bar{\gamma}_0^0(t)) \cdot (0, -1)^T dt.$$

Proof. As in the proof of [12, Proposition 2.3], we consider a projectivisation of the flow of (11); however, due to the z -dependence of Equation (11b), we cannot *a priori* discount the $\mathcal{O}(\varepsilon)$ -correction to the reduced flow on \mathcal{S}_0^{a+} in our case. Hence, we write $z = z(v, w, \varepsilon) = Z_0(v) + \varepsilon Z_1(v, w) + \mathcal{O}(\varepsilon^2)$, where $Z_0(v) = -v^3 + \sqrt{3}v^2 = f(v)$. Substituting the above Ansatz into (11b), noting that $\dot{z} = \frac{\partial Z_0}{\partial v} \dot{v} + \varepsilon \left(\frac{\partial Z_1}{\partial v} \dot{v} + \frac{\partial Z_1}{\partial w} \dot{w} \right) + \mathcal{O}(\varepsilon^2)$, and making use of Equation (11a), we find

$$Z_1(v, w) = -\frac{v - w - \kappa f(v)}{f'(v)} = -\frac{v - w - \kappa(\sqrt{3}v^2 - v^3)}{2\sqrt{3}v - 3v^2}.$$

Since, moreover, $\dot{z} = \left(\frac{\partial Z_0}{\partial v} + \varepsilon \frac{\partial Z_1}{\partial v} \right) \dot{v} + \mathcal{O}(\varepsilon\sqrt{\varepsilon})$, as $\frac{\partial Z_1}{\partial v} = \mathcal{O}(1)$ and $\frac{\partial Z_1}{\partial w} = \mathcal{O}(\varepsilon^{-\frac{1}{2}})$ for $v \in [-\rho, -\alpha\sqrt{\varepsilon}]$ and $w = \mathcal{O}(\varepsilon)$, while $\dot{w} = \mathcal{O}(\varepsilon)$ due to Equation (11c), a straightforward calculation yields the following projection of (11a) onto the slow manifold $\mathcal{S}_\varepsilon^{a+}$:

$$[2\sqrt{3}v - 3v^2 + \mathcal{O}(\varepsilon)]\dot{v} = v - w - \kappa \left[\sqrt{3}v^2 - v^3 - \varepsilon \frac{v - w - \kappa(\sqrt{3}v^2 - v^3)}{2\sqrt{3}v - 3v^2} \right] + \varepsilon(v + w) + \mathcal{O}(\varepsilon\sqrt{\varepsilon}).$$

The corresponding projected system on $\mathcal{S}_\varepsilon^{a+}$ that is obtained from (11) is then given by

$$(26a) \quad \dot{v} = -\left\{ v - w - \kappa \left[\sqrt{3}v^2 - v^3 - \varepsilon \frac{v - w - \kappa(\sqrt{3}v^2 - v^3)}{2\sqrt{3}v - 3v^2} \right] + \varepsilon(v + w) \right\},$$

$$(26b) \quad \dot{w} = -\varepsilon \kappa (\mu - w - v) (2\sqrt{3}v - 3v^2)$$

after desingularisation, *i.e.*, multiplication with a factor of $-\frac{\partial z}{\partial v} = -[2\sqrt{3}v - 3v^2 + \mathcal{O}(\varepsilon)]$, which is certainly positive for ε sufficiently small and $v \leq -\alpha\sqrt{\varepsilon}$, as above. (Here, we have neglected the resulting $\mathcal{O}(\varepsilon^2)$ -correction in (26b), as well as terms of order $\mathcal{O}(\varepsilon\sqrt{\varepsilon})$ and upwards in (26a), as both are irrelevant to the order considered here.)

Next, we define the new (projective) variable $W = \frac{w}{v}$, and we rewrite Equation (26) in terms of W to obtain

$$(27a) \quad \dot{v} = -v\mathcal{F}(v, W, \kappa, \varepsilon),$$

$$(27b) \quad \dot{W} = W\mathcal{F}(v, W, \kappa, \varepsilon) - \varepsilon \kappa (\mu - vW - v) [2\sqrt{3} - 3v + \mathcal{O}(\sqrt{\varepsilon})].$$

Since the function \mathcal{F} , which is defined as

$$\mathcal{F}(v, W, \kappa, \varepsilon) = 1 - W - \kappa \left[\sqrt{3}v - v^2 - \varepsilon \frac{1 - W - \kappa(\sqrt{3}v - v^2)}{2\sqrt{3}v - 3v^2} \right] + \varepsilon(1 + W),$$

is non-zero – and, in fact, positive – for $(v, W, \kappa, \varepsilon)$ sufficiently small, we may perform a transformation of time in Equation (27) to cancel a factor of \mathcal{F} from the right-hand sides therein. (Without

loss of generality, and with an abuse of notation, we again denote the new rescaled time by τ .) Next, we expand the resulting equations, taking into account that

$$Z_1(v, W) \equiv Z_1(v, vW) = \frac{1}{2v} \left[\frac{\sqrt{3}}{3} - \left(\kappa - \frac{1}{2} \right) v + \mathcal{O}(v^2) \right],$$

to leading order in W , and noting that $W = \mathcal{O}(\sqrt{\varepsilon})$ due to $v \in [-\rho, -\alpha\sqrt{\varepsilon}]$ and $w = \mathcal{O}(\varepsilon)$. Neglecting terms of second order and upwards in (v, W) , we thus have the following approximation for (27), which is analogous to [12, Equation (2.25)]:

$$(28a) \quad \dot{v} = -v,$$

$$(28b) \quad \dot{W} = (1 - 2\sqrt{3}\kappa\mu\varepsilon)W - 2\sqrt{3}\kappa\mu\varepsilon + (3\mu + 2\sqrt{3} - 6\kappa\mu)\kappa\varepsilon v.$$

Since Equation (28a) can be integrated explicitly, with $v(\tau) = -\rho e^{-\tau}$, we may substitute into (28b) and solve for $W(\tau)$; given the (rescaled) transition time $T = \ln \frac{\rho}{\alpha\sqrt{\varepsilon}}$ between Σ^{in} and Δ^{in} , we then evaluate the resulting solution to obtain

$$W(T) = \frac{\rho}{\alpha\sqrt{\varepsilon}} W^{\text{in}} (1 + \sqrt{3}\kappa\mu\varepsilon \ln \varepsilon) + \mathcal{O}(\sqrt{\varepsilon}),$$

as sketched in Figure 5(a). Finally, we make use of the fact that $w(T) = -\alpha\sqrt{\varepsilon}W(T)$, as well as of $w^{\text{in}} = -\rho W^{\text{in}}$, to find $w(T) = w^{\text{in}}(1 + \sqrt{3}\kappa\mu\varepsilon \ln \varepsilon) + \mathcal{O}(\varepsilon)$.

It remains to consider the transition from $\bar{\Delta}^{\text{in}}$ to $\bar{\Delta}_-$; in analogy to [12], we denote the corresponding map by $\bar{\Pi}^{\text{in}}$. To that end, we recall the proof of Proposition 1 from the previous subsection, taking into account that we need to transform between original and rescaled (‘blown-up’) coordinates; cf. Equation (13). Then, it is easy to see that

$$(29) \quad (h^-, \bar{w}^-) = \bar{\Pi}(\bar{z}, \bar{w}) = (\sqrt{\varepsilon}d_{\sqrt{\varepsilon}}^- + \bar{w}d_{\bar{w}}^- + \mathcal{O}[(\sqrt{\varepsilon} + \bar{w})^2], \bar{w} + 2\sqrt{3}\alpha\kappa\mu\varepsilon + \mathcal{O}(\varepsilon^2)),$$

where $d_{\sqrt{\varepsilon}}^-$ and $d_{\bar{w}}^-$ are defined as in the statement of the proposition; see also [12, Equation (2.30)]. (In particular, one observes that these coefficients correspond to the solution curve $\bar{\gamma}_0^0$ defined in Equation (17), as well as that the transition time between $\bar{\Delta}^{\text{in}}$ and $\bar{\Delta}_-$ is given by $\bar{T}^{\text{in}} = 2\sqrt{3}\alpha$, as in [12].)

Finally, we combine the estimate for \bar{w}^- in (29) with the asymptotics of $w(T)$ derived above, noting that the condition for $(\bar{v}, \bar{z}, \bar{w})$ to lie on a trajectory originating in $\mathcal{S}_\varepsilon^{a+}$ is, in fact, expressed by the h^- -component of $\bar{\Pi}(\bar{z}, \bar{w})$. Taking into account that $\bar{w} = \frac{w}{\sqrt{\varepsilon}}$, we obtain Equation (25), as claimed. \square

We remark that the term $\frac{w^{\text{in}}}{\sqrt{\varepsilon}}$ in (25) remains bounded as $\varepsilon \rightarrow 0^+$, since $w^{\text{in}} = \mathcal{O}(\varepsilon)$ by Assumption 1; hence, $(h^-, \bar{w}^-) \rightarrow (0, 0)$ in that limit, which is consistent with the definition of the singular solution $\bar{\gamma}_0^0$.

Remark 5. It follows from the first part of the proof of Proposition 2 that the flow between Σ^{in} and Δ^{in} can, in fact, be approximated by the reduced dynamics on the critical manifold \mathcal{S}_0^{a+} , as was also done in [12, Proposition 2.3]. (Specifically, our expression for $w(T)$ agrees with the one obtained there, *i.e.*, the $\mathcal{O}(\varepsilon)$ -correction due to Z_1 turns out to be irrelevant *a posteriori*.) Similarly, the second part of that proof implies that our approximation of the transition between $\bar{\Delta}^{\text{in}}$ and $\bar{\Delta}_-$ via the singular (integrable) system in (15) is sufficiently accurate, as the resulting \bar{T}^{in} -dependent correction to \bar{w}^- does not even enter Equation (25) to the order considered here. \square

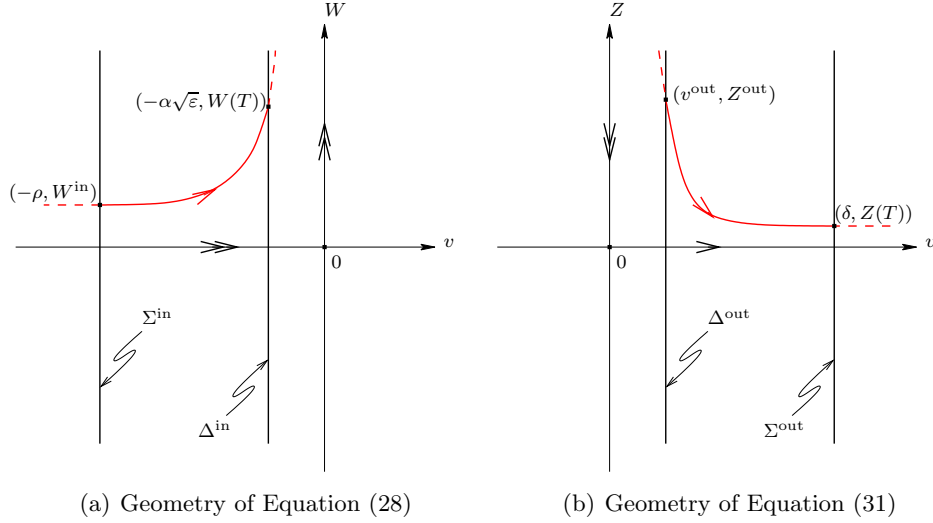


FIGURE 5. Illustration of entry and exit mechanisms.

3.1.3. *Exit mechanism.* As in the previous subsection, the analysis of the exit from the fold region is divided into two portions: first, we consider the transition between the section $\bar{\Delta}_-$ and its image under the flow of (14) at time $T^{h,\text{out}}(\bar{w}) := -T_-^{-h}(\bar{w})$, which we denote by $\bar{\Delta}^{\text{out}}$; then, we study the transition from $\bar{\Delta}^{\text{out}}$ to the section Σ^{out} defined in Section 2.4. (Naturally, we are interested in $h < 0$ here, since trajectories with $h > 0$ cannot leave the fold region, as noted in Section 3.1.1.)

We require the following notation: we write C_ε^a and C_ε^r for the intersection curves of $\mathcal{S}_\varepsilon^{a+}$ and $\mathcal{S}_\varepsilon^r$ with the Poincaré section Δ that was defined in Section 3.1.1. (Here, we remark that these curves were denoted by C_ε^\pm in [12]; however, due to the fact that the canard phenomenon is observed at ℓ^+ instead of at ℓ^- in our case, recall Section 2, we had to adapt our notation accordingly.) Finally, as in [12, Section 2.4], we introduce a change of variable in \bar{z} such that the curve C_ε^r becomes parallel to the \bar{w} -axis in $\bar{\Delta}$ when written in terms of the new variable \tilde{z} :

Proposition 3. *Let $(h, \bar{w}) \in \bar{\Delta}_-$, with $h < 0$ and $h = \mathcal{O}(\varepsilon^M)$ for some $M > 0$, and let $\varepsilon \in [0, \varepsilon_0]$ be sufficiently small. Then, the transition map $\Pi^{\text{out}} : \bar{\Delta}_- \rightarrow \Sigma^{\text{out}}$ is of the form*

$$(30) \quad (z^{\text{out}}, w^{\text{out}}) := \Pi^{\text{out}}(h, \bar{w}) = (\varepsilon \tilde{z}^{\text{out}} + \mathcal{O}(\varepsilon \ln \varepsilon), \sqrt{\varepsilon} \bar{w} + \varepsilon \sqrt{\varepsilon} \kappa \mu T^{h,\text{out}}(\bar{w}) + \mathcal{O}(\varepsilon \sqrt{\varepsilon})),$$

where \tilde{z}^{out} is the \tilde{z} -value corresponding to $h^{\text{out}} = h + \sqrt{\varepsilon} d_{\sqrt{\varepsilon}}^{\text{out}} + \bar{w} d_{\bar{w}}^{\text{out}}$, with

$$d_{\sqrt{\varepsilon}}^{\text{out}} = - \int_0^{T^{h,\text{out}}(\bar{w})} \nabla H(\bar{\gamma}_0^h(t)) \cdot (-\bar{v}_0^h(t)^3, -\kappa \bar{z}_0^h(t))^T dt$$

and

$$d_{\bar{w}}^{\text{out}} = - \int_0^{T^{h,\text{out}}(\bar{w})} \nabla H(\bar{\gamma}_0^h(t)) \cdot (0, -1)^T dt.$$

Proof. As the proof is very similar to that of [12, Proposition 2.4], we merely sketch it here, emphasising the requisite modifications.

Let $(h, \bar{w}) \in \bar{\Delta}_-$, and let $\bar{\Pi}^{\text{out}}$ denote the time- $T^{h,\text{out}}(\bar{w})$ transition map between $\bar{\Delta}_-$ and the (implicitly defined) section $\bar{\Delta}^{\text{out}} := \bar{\Pi}^{\text{out}}(\bar{\Delta}_-)$. Then, it follows immediately from the near-integrability of Equation (14) that

$$(h^{\text{out}}, \bar{w}^{\text{out}}) := \bar{\Pi}^{\text{out}}(h, \bar{w}) = (h + \sqrt{\varepsilon} d_{\sqrt{\varepsilon}}^{\text{out}} + \bar{w} d_{\bar{w}}^{\text{out}} + \mathcal{O}[(\sqrt{\varepsilon} + \bar{w})^2], \bar{w} + \varepsilon \kappa \mu T^{h,\text{out}}(\bar{w}) + \mathcal{O}(\varepsilon \sqrt{\varepsilon})),$$

where $d_{\sqrt{\varepsilon}}^{\text{out}}$ and $d_{\bar{w}}^{\text{out}}$ are defined as in the statement of the proposition; see also the proof of Proposition 1.

The second part of the transition – from $\bar{\Delta}^{\text{out}}$ to Σ^{out} – is studied via a change of variables, with $z = v^2 Z$, which can be considered as a ‘phase-directional’ chart in ‘blown-up’ phase space; see again [12] for details. Rewriting (12) in terms of (v, Z, w) and rescaling time by dividing out a (positive) factor of $\Phi(v, Z) = v^2(-Z + \sqrt{3} - v)$ from the right-hand sides of the resulting equations, we obtain

$$(31a) \quad v' = 1,$$

$$(31b) \quad Z' = -2\frac{Z}{v} + \frac{\varepsilon}{v\Phi(v, Z)} \left[1 - \frac{w}{v} - \kappa v Z + \varepsilon \left(1 + \frac{w}{v} \right) \right],$$

$$(31c) \quad w' = \frac{\varepsilon^2}{\Phi(v, Z)} \kappa(\mu - w - v).$$

(With an abuse of notation, the prime now denotes differentiation with respect to the new, rescaled time.) To leading order, Equations (31a) and (31b) are identical to [12, Equations (2.45a) and (2.45b)]. Also, as there, $v^{\text{out}} = \mathcal{O}(\sqrt{\varepsilon}T^{h,\text{out}}) = \mathcal{O}(\sqrt{-\varepsilon \ln \varepsilon})$ and $w = \mathcal{O}(\varepsilon)$ imply $\frac{w}{v} = \mathcal{O}(\sqrt{\varepsilon})$ and $\frac{dw}{dt} = \mathcal{O}(\varepsilon(\ln \varepsilon)^{-1})$. Expanding Φ , we then find $Z' = -\frac{2}{v}Z + \frac{\varepsilon}{v^3}\frac{\sqrt{3}}{3}[1 - \kappa v Z + \mathcal{O}(v, Z)]$; moreover, as $vZ = \mathcal{O}(1)$, we obtain $z(T) = \varepsilon \tilde{z}^{\text{out}} + \mathcal{O}(\varepsilon \ln \varepsilon)$ for the corresponding leading-order solution, in analogy to [12]. (Here, T denotes the transition time from Δ^{out} to Σ^{out} , as illustrated in Figure 5(b).)

It remains to consider the evolution of w : to that end, we integrate Equation (12c) directly. Expanding the solution and noting that $T \leq \frac{2\sqrt{3}}{3v^{\text{out}}} + \frac{1}{3} \ln \varepsilon + \mathcal{O}(1)$, again by [12], we deduce

$$\begin{aligned} w(T) &= \sqrt{\varepsilon} \bar{w}^{\text{out}} + \varepsilon^2 \left(\kappa \mu T - \sqrt{\varepsilon} \kappa \bar{w}^{\text{out}} T + \int_{v^{\text{out}}}^{\delta} \frac{v}{\Phi(v, 0)} dv \right) + \mathcal{O}(\varepsilon^3) \\ &= \sqrt{\varepsilon} \bar{w} + \varepsilon \sqrt{\varepsilon} \kappa \mu T^{h,\text{out}}(\bar{w}) + \mathcal{O}(\varepsilon \sqrt{\varepsilon}). \end{aligned}$$

(As in the proof of [12, Proposition 2.4], one easily sees that the integral term in the above expression is of higher order, by combining the fact that $\int \frac{v}{\Phi(v, 0)} dv = -\frac{\sqrt{3}}{3} \ln \frac{v}{\sqrt{3}+v} + c$ with the asymptotics of v^{out} .) Finally, collecting the above estimates, we have Equation (30), as claimed. \square

3.2. Return map Π . In this subsection, we approximate the ‘composite’ return map Π that is induced by the flow of (11) in the three time-scale regime considered here: combining the asymptotic formulae for Π^{ret} , $\bar{\Pi}$, Π^{in} , and Π^{out} , as obtained in Lemma 2 and Propositions 1 through 3, respectively, we may write

$$(32) \quad \Pi(h, \bar{w}) = \begin{cases} \bar{\Pi}(h, \bar{w}) & \text{if } h > 0, \\ \Pi^{\text{in}} \circ \Pi^{\text{ret}} \circ \Pi^{\text{out}}(h, \bar{w}) & \text{if } h < 0; \end{cases}$$

for future reference, we note that Π is defined as a Poincaré map from Δ_- – or, rather, its ‘blown-up’ analogue $\bar{\Delta}_-$ – to itself.

Obviously, the definition of Π thus depends on the sign of h : for positive h , the point of intersection of the corresponding trajectory with Δ lies above $\mathcal{C}_\varepsilon^r$, forcing the flow back into the fold region; for negative h , on the other hand, that point lies below $\mathcal{C}_\varepsilon^r$, allowing the trajectory to leave and undergo relaxation. Correspondingly, in the resulting time series, one hence obtains an SAO in the former case and an LAO in the latter; since, moreover, the sign of h may change after each application of Π , iteration of the above procedure generates the mixed-mode patterns that are observed in Equation (11). A cartoon illustration of how the segment 1^2 – in which two SAOs are followed by one LAO – is produced by iterating Π can be found in Figure 6.

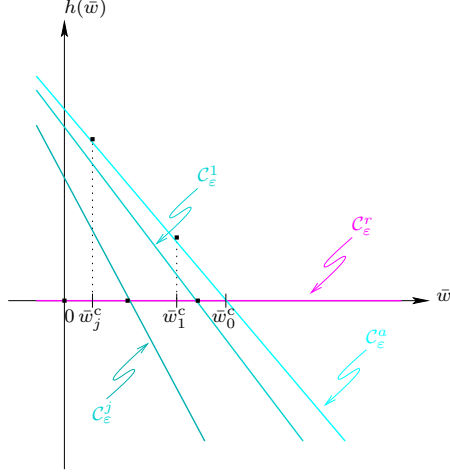


FIGURE 7. Curves $\mathcal{C}_\varepsilon^j$ for $j \geq 0$.

3.2.1. *Derivative of Π .* Given Equation (33), we immediately conclude that

$$(34) \quad \frac{d\Pi}{d\bar{w}} \sim \begin{cases} 1 + \varepsilon\kappa\mu \frac{dT^{h^j(\bar{w})}(\bar{w})}{d\bar{w}} & \text{if } h^j(\bar{w}) > 0, \\ 1 + \varepsilon\kappa\mu \frac{dT^{h^j(\bar{w}),\text{out}}(\bar{w})}{d\bar{w}} & \text{if } h^j(\bar{w}) < 0, \end{cases}$$

to leading order in ε . Estimates for the derivatives of the transition times $T^{h^j(\bar{w})}$ and $T^{h^j(\bar{w}),\text{out}}$ can be obtained verbatim as in [12, Section 3.2], as they are based on the asymptotics of the near-integrable system in (14). (Here, we recall that the only difference to the corresponding Equation (2.3) in [12], to the order considered here, is due to the \bar{z} -dependence of (14b). Thus, the definition of the coefficient $d_{\sqrt{\varepsilon}}^h$ includes an additional contribution from \bar{z}_0^h in our case; cf. Equation (20).) In sum, we thus find

$$\frac{dT^{h^j(\bar{w})}(\bar{w})}{d\bar{w}} \sim -\frac{2}{h^j(\bar{w})} \frac{1}{\sqrt{-2 \ln h^j(\bar{w})}} (j+1) d_{\bar{w}}^0$$

and

$$\frac{dT^{h^j(\bar{w}),\text{out}}(\bar{w})}{d\bar{w}} \sim \frac{1}{h^j(\bar{w})} \frac{1}{\sqrt{-2 \ln h^j(\bar{w})}} (j+1) d_{\bar{w}}^0.$$

3.3. Secondary canards and sectors of rotation. Following [12, Section 1], we define the *strong canard* Γ_ε ($\equiv \Gamma_\varepsilon^0$) as the trajectory of Equation (12) which lies in the transverse intersection of the attracting sheet $\mathcal{S}_\varepsilon^{a+}$ and the repelling sheet $\mathcal{S}_\varepsilon^r$ of the slow manifold \mathcal{S}_ε , for ε positive and sufficiently small. (As discussed in Section 3.1.1, Γ_ε is to lowest order described by the ‘special’ solution $\bar{\gamma}_0^0$ in the fold region, cf. (17), which organises the flow of the rescaled Equation (14) in the singular limit.) Clearly, the strong canard corresponds to a ‘critical’ value \bar{w}_0^c of \bar{w} which equals, in fact, the \bar{w} -coordinate of the point of intersection of the curves $\mathcal{C}_\varepsilon^a$ and $\mathcal{C}_\varepsilon^r$ defined in Section 3.2; details can be found in [12, Section 1]. Similarly, for $j \geq 1$, we may define \bar{w}_j^c as the \bar{w} -coordinate of the point of intersection of $\mathcal{C}_\varepsilon^j$ with $\mathcal{C}_\varepsilon^r$; see again Figure 7. The corresponding trajectory of (12) is called the *j*th *secondary canard* Γ_ε^j , and undergoes *j* SAOs (‘loops’) in the fold region before relaxation; recall Figure 1, where the trajectories Γ_ε^j are sketched for $j = 0, 1$. Correspondingly, we call the \bar{w} -interval $(\bar{w}_j^c, \bar{w}_{j-1}^c)$ the *j*th *sector of rotation*, and we denote it by RS^j [12, Section 3.3].

To estimate \bar{w}_0^c to leading order in ε , we follow [12], demanding that $\hat{h} = h$; recall Proposition 1. Approximating $\pm T^h \sim \pm T^0 = \pm\infty$ in Equations (20) and (21) and evaluating ∇H at γ_0^0 , as defined in (17), we find $d_{\sqrt{\varepsilon}}^0 = \frac{1}{48}(1+2\kappa)\sqrt{2\pi e}$ and $d_{\bar{w}}^0 = -\frac{1}{2\sqrt{3}}\sqrt{2\pi e}$ – see also [12, Equation (2.18)] – and, hence,

$$(35) \quad \bar{w}_0^c = -\frac{d_{\sqrt{\varepsilon}}^0}{d_{\bar{w}}^0}\sqrt{\varepsilon} + \mathcal{O}(\varepsilon) = \frac{\sqrt{3}}{24}(1+2\kappa)\sqrt{\varepsilon} + \mathcal{O}(\varepsilon).$$

Numerical simulation (data not shown) suggests excellent agreement with the above estimate for \bar{w}_0^c , even for the ‘large’ value of $\varepsilon = 0.1$ considered here. (Specifically, taking $\kappa = 0.35$, as before, we find $\bar{w}_0^c \sim \frac{2651}{68330}\sqrt{3} \approx 0.03880$.)

The other key quantity of interest, apart from the critical value \bar{w}_0^c of \bar{w} , concerns the width of the sectors of rotation RS^j , as defined above. To obtain the corresponding estimate, we need to account for additional terms in the expansion for the transition map $\bar{\Pi}$ introduced in Section 3.1.1. (In fact, by combining the resulting two estimates, we may approximate the critical \bar{w} -values $\{\bar{w}_j^c\}$ for $j = 1, \dots, k$.)

Thus, we now consider the partially decoupled truncated system of equations

$$(36a) \quad \bar{v}' = \sqrt{3}\bar{v}^2 - \bar{z} - \sqrt{\varepsilon}\bar{v}^3 + \sqrt{\varepsilon}F(0,0) + \bar{w}G(0,0),$$

$$(36b) \quad \bar{z}' = \bar{v} - \bar{w} - \kappa\sqrt{\varepsilon}\bar{z} + \varepsilon(\bar{v} + \bar{w}),$$

$$(36c) \quad \bar{w}' = \varepsilon\kappa\mu,$$

which is defined in analogy to [12, Equation (3.15)]. We note that Equation (36) differs from the ‘rescaled’ system in (14) in two points: first, $\bar{w}(t)$ is not assumed to be constant; rather, Equation (14c) is approximated by $\bar{w}' \sim \varepsilon\kappa\mu$, which yields $\bar{w}(t) \sim \bar{w} + \varepsilon\kappa\mu t$ after integration, where \bar{w} is some initial value. Second, the inclusion of higher-order terms in $\sqrt{\varepsilon}$ and \bar{w} in the \bar{v} -equation – which are multiplied by appropriately defined functions $F(\bar{w}, \sqrt{\varepsilon})$ and $G(\bar{w}, \sqrt{\varepsilon})$, respectively, that are, to leading order, evaluated at $(\bar{w}, \sqrt{\varepsilon}) = (0,0)$ – is due to the transformation to the new variable \bar{z} ; see Section 3.1.3 and [12, Proposition 2.4] for details.

Finally, let $\bar{\Pi}_0$ denote the ‘reduced’ transition map for the system that is obtained by appending $\bar{w}' = 0$ to Equations (36a) and (36b). Then, one has the following result; cf. also [12, Proposition 3.2]:

Proposition 4. *Let $\bar{\Pi} : \bar{\Delta}_- \rightarrow \bar{\Delta}_-$ denote the return map for (14), and let $\varepsilon \in [0, \varepsilon_0]$ be sufficiently small. Then,*

$$(37) \quad \bar{\Pi}(h, \bar{w}) = \begin{pmatrix} P_h \bar{\Pi}_0(h, \bar{w}) + \varepsilon\kappa\mu\mathcal{K}(h) + \mathcal{O}(\varepsilon\sqrt{\varepsilon}) \\ \bar{w} + 2\varepsilon\kappa\mu T^h + \mathcal{O}(\varepsilon\sqrt{\varepsilon}) \end{pmatrix},$$

where P_h is the projection onto the \bar{h} -coordinate, with $P_h \bar{\Pi}_0(h, \bar{w}) = \hat{h}$ as in Proposition 1, and

$$\mathcal{K}(h) = \int_{-T^h}^{T^h} \nabla H(\bar{\gamma}_0^h(t)) \cdot (G(0,0), -1)^T (t + T^h) dt.$$

(In particular, one can show that $\mathcal{K}(h) = 2d_{\bar{w}}^0 T^h + \mathcal{O}(1)$, where $d_{\bar{w}}^0$ is defined as in Equation (21); see [12, Lemma A.5].)

Proof. As in the proof of [12, Proposition 3.2], one considers the partially decoupled truncated equations

$$(38) \quad \begin{aligned} \bar{v}' &= \sqrt{3}\bar{v}^2 - \bar{z} - \sqrt{\varepsilon}\bar{v}^3 + \sqrt{\varepsilon}F(0,0) + (\bar{w} + \varepsilon\kappa\mu t)G(0,0), \\ \bar{z}' &= \bar{v} - \bar{w} - \varepsilon\kappa\mu t - \kappa\sqrt{\varepsilon}\bar{z} + \varepsilon(\bar{v} + \bar{w} + \varepsilon\kappa\mu t). \end{aligned}$$

Since the above system agrees with [12, Equation (3.17)] to leading order – apart from the additional $\kappa\sqrt{\varepsilon}\bar{z}$ -term, which, however, only affects the definition of $d_{\sqrt{\varepsilon}}^h$, as seen in the proof of Proposition 1 – we find

$$P_h\bar{\Pi} \sim P_h\bar{\Pi}_0 + \varepsilon\kappa\mu\mathcal{K}(h) + \varepsilon \int_{-T^h}^{T^h} \nabla H(\bar{\gamma}_0^h(t)) \cdot (0, \bar{v}_0^h) dt.$$

Here, we have neglected terms of second order and upwards in (ε, \bar{w}) ; moreover, we note that any contribution coming from terms involving $F(0, 0)$ and $G(0, 0)$ evaluates to zero by symmetry: as in the proof of [12, Proposition 2.2], we have $(\bar{v}_0^h, \bar{z}_0^h)(-t) = (-\bar{v}_0^h, \bar{z}_0^h)(t)$ on $\bar{\gamma}_0^h$. Finally, making again use of the oddness of \bar{v}_0^h , one can show that the integral term in the above expression vanishes. In sum, one hence obtains the refined expansion for $\bar{\Pi}$ in Equation (37), as claimed, which completes the proof. \square

Given the result of Proposition 4, as well as Equation (18), one can show as in [12, Proposition 3.3] that the width of the j th sector of rotation RS^j is approximately given by

$$(39) \quad \Delta\bar{w} := \bar{w}_j^c - \bar{w}_{j-1}^c \sim -2\varepsilon\kappa\mu\sqrt{-2\ln\varepsilon}.$$

The above estimate is confirmed by numerical simulation (data not shown) and implies, in particular, that all sectors of rotation are of the same width to leading order for ε fixed, as well as that the sector RS^j is located ‘to the left’ of RS^{j-1} for any $j \geq 1$ due to $\Delta\bar{w} < 0$; see [12, Section 3.3] for details. (Undoing the rescaling in (13), one finds $\Delta w = \mathcal{O}(\varepsilon\sqrt{-\varepsilon\ln\varepsilon})$ for the corresponding estimate in terms of the original w -variable.) Consequently, it follows again as in [12, Section 3.3] that we will always observe a finite number of SAOs in any mixed-mode time series of (12); cf. also Section 4 below.

3.4. Reduced return map Φ . The final step in our analysis of the return map Π consists in a further reduction to a simplified, one-dimensional map $\Phi : \mathcal{C}_\varepsilon^a \rightarrow \mathcal{C}_\varepsilon^a$, which can be defined as follows [12, Section 3.4]: for $k \geq 0$,

$$\Phi(\bar{w}) = P_{\bar{w}}(\Pi^{\text{in}} \circ \Pi^{\text{ret}} \circ \Pi^{\text{out}} \circ \bar{\Pi}^k(h^0(\bar{w}), \bar{w})) \quad \text{if } (h^0(\bar{w}), \bar{w}) \in RS^k.$$

(Here, $P_{\bar{w}}$ denotes the projection onto the \bar{w} -coordinate, as before.) While the map Φ is hence defined on the single curve $\mathcal{C}_\varepsilon^a$ instead of on a union of curves $\bigcup \mathcal{C}_\varepsilon^j$, and while it is unimodal on each of the sectors of rotation RS^k , it has discontinuities at the boundaries between these sectors. The dynamics of Φ was studied in detail in Section 3.6 of [12]; here, we merely sketch the derivation of some of its properties that are relevant to us.

One such property concerns the derivative of Φ (with respect to \bar{w}) on RS^k ; the resulting estimate will allow us to characterise the contraction, or expansion, under Φ . Making use of the definition of Π^{in} , Π^{ret} , Π^{out} , and $\bar{\Pi}$, in combination with the Chain Rule and the fact that $h^j(\bar{w}^j) = \mathcal{O}(\varepsilon\sqrt{-\ln\varepsilon})$, we conclude as in [12, Lemma 3.5] that

$$(40) \quad \Phi'(\bar{w}) = 1 - \varepsilon\kappa\mu d_{\bar{w}}^0 \frac{1}{\sqrt{-2\ln\varepsilon}} \left(\sum_{j=0}^{k-1} \frac{2(j+1)}{h^j(\bar{w}^j)} + \frac{k+1}{h^k(\bar{w}^k)} \right) \sim 1 - \frac{\omega_k(\nu)}{4\ln\varepsilon};$$

see, in particular, [12, Equations (3.32) and (3.33)]. Here, \bar{w}^j is the j th iterate of some initial \bar{w} -value \bar{w}^0 under $\bar{\Pi}$, and the auxiliary function ω_k is defined as

$$\omega_k(\nu) = \sum_{j=0}^{k-1} \frac{1}{k-j-\nu} - \frac{1}{2\nu},$$

where $\nu \in [0, 1]$ for $k \geq 1$, while $\nu > 0$ when $k = 0$.

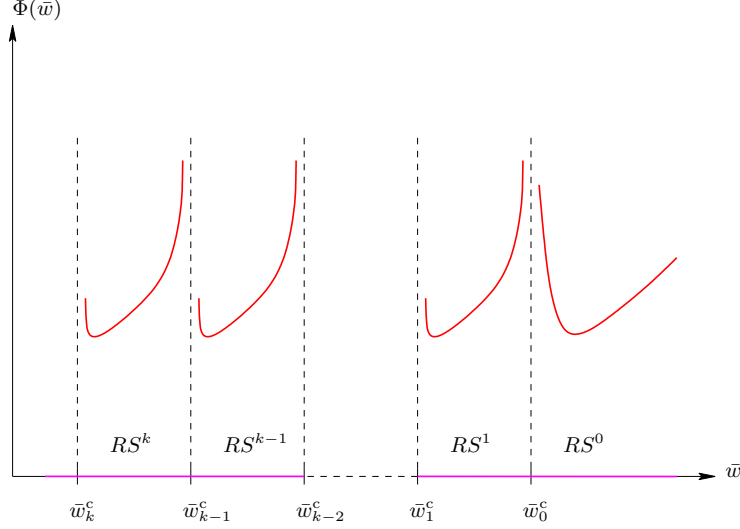


FIGURE 8. Reduced return map Φ .

Given the above estimate for Φ' , one can, for instance, show that the map Φ has a (local) minimum in each sector RS^k , *i.e.*, at some \bar{w} -value \bar{w}_{\min}^k . Moreover, one may write $\Phi(\bar{w}_{\min}^k) = \Phi_{\min} + \mathcal{O}(\varepsilon)$, with

$$\begin{aligned} \Phi_{\min} &\sim \bar{w}_0^c + \sqrt{\varepsilon} [\mathcal{G}(v_0, v_{\max}, \mu) + \mathcal{G}(v_{\max}^*, 0, \mu)] + \varepsilon \kappa \mu T^{h(\bar{w}_{\min}^0), \text{out}} \\ &\sim \sqrt{\varepsilon} \left[3\kappa \left(1 - \frac{1}{2}\kappa \right) \mu - \frac{1}{2} \sqrt{3} \left(\kappa^2 - \frac{1}{6}\kappa - \frac{1}{12} \right) \right] + \varepsilon \kappa \mu \sqrt{-2 \ln \varepsilon}; \end{aligned}$$

recall Equations (35), (7), (33), and (18), where the latter implies, in particular, $T^h \sim \sqrt{-2 \ln \varepsilon}$. Hence, it follows that Φ assumes the same minimum value (to leading order) for any $k = 0, 1, 2, \dots$; cf. [12, Equation (3.36)]. A qualitative illustration of the map Φ is given in Figure 8.

Next, we investigate the existence and stability of ‘regular’ mixed-mode periodic orbits with signature 1^k ; specifically, we estimate the width of the corresponding μ -interval $(\underline{\mu}^k, \bar{\mu}^k)$. In analogy to [12, Theorem 3.7], we obtain

Proposition 5. *Let $K > 0$ be arbitrary, but fixed; then, there is some (small) $\varepsilon_0 > 0$ such that, for $k = 1, \dots, K$ and $\varepsilon \in [0, \varepsilon_0]$, the periodic orbit of type 1^k exists and is stable when $\mu \in (\underline{\mu}^k, \bar{\mu}^k)$, with*

$$(41) \quad \Delta \mu^k := \bar{\mu}^k - \underline{\mu}^k \sim -\frac{\underline{\mu}^k \kappa}{\sqrt{2} D_\mu} \frac{\sqrt{\varepsilon}}{\sqrt{-\ln \varepsilon}} \int_{\nu_{-2}^k}^{\nu_0^k} \omega_k(\nu) d\nu.$$

Here, ν_{-2}^k and ν_0^k are defined by $\omega_k(\nu_{-2}^k) = 8 \ln \varepsilon$ and $\omega_k(\nu_0^k) = 0$, respectively, and

$$D_\mu = \frac{d}{d\mu} [\mathcal{G}(v_0, v_{\max}, \mu) + \mathcal{G}(v_{\max}^*, 0, \mu)]$$

is found by differentiating Equation (7) with respect to μ .

Proof. The proof of Equation (41) is based on the observation that periodic orbits with signature 1^k correspond to fixed points of Φ , *i.e.*, to solutions of $\Phi(\bar{w}, \mu) = \bar{w}$. The stability of those points follows from the second estimate for Φ' in Equation (40), as one can show that $|\Phi'(\bar{w}, \mu)| < 1$ if and

only if $\nu \in (\nu_{-2}^k, \nu_0^k)$ in ω_k , with ν_{-2}^k and ν_0^k as defined above. Implicit differentiation then gives

$$\frac{d\mu}{d\bar{w}} = -\frac{\frac{\partial}{\partial \bar{w}}\Phi(\bar{w}, \mu) - 1}{\frac{\partial}{\partial \mu}\Phi(\bar{w}, \mu)} \sim \frac{\frac{1}{4\ln \varepsilon}\omega_k(\nu)}{D_\mu\sqrt{\varepsilon}};$$

here, we have again used (40) as well as the estimate $\frac{\partial}{\partial \mu}\Phi(\bar{w}, \mu) \sim D_\mu\sqrt{\varepsilon}$.

Finally, applying the Fundamental Theorem of Calculus, we find

$$\Delta\mu^k = \int_{\bar{w}(\mu^k)}^{\bar{w}(\bar{\mu}^k)} \frac{d\mu}{d\bar{w}} d\bar{w} \sim \frac{\Delta\bar{w}^k}{4D_\mu\sqrt{\varepsilon}\ln \varepsilon} \int_{\nu_{-2}^k}^{\nu_0^k} \omega_k(\nu) d\nu.$$

Approximating $\Delta\bar{w}^k$ by $\Delta\bar{w} \sim -2\varepsilon\kappa\mu\sqrt{-2\ln \varepsilon}$, recall Equation (39), we obtain (41), as claimed. \square

(The restriction to $k \leq K$ in the statement of Proposition 5 is due to the fact that our asymptotics is not uniform in k with respect to ε ; see [12, Proposition 3.4].) Since the remainder of the analysis presented in [12, Section 3.6] carries over *mutatis mutandis* to the context of Equation (12), we do not retrace it here. Rather, we emphasise that the resulting mixed-mode dynamics, which will be discussed in detail in Section 4 below, is qualitatively equivalent to that of the canonical Equation (2).

4. DISCUSSION

In this article, we have studied mixed-mode oscillatory behaviour in a three-dimensional extended Bonhoeffer-van der Pol oscillator whose dynamics evolves on three distinct time-scales, thus complementing results previously obtained in [18]. To that end, we have transformed the governing equations into a form that is close to a simplified ‘prototypical’ model system which was proposed by Krupa *et al.* [12]; in the process, we have identified one bifurcation parameter that unfolds the mixed-mode dynamics generated by Equation (1), expressing it as a function of two of the original parameters in the system. (An alternative approach, which was suggested recently [16] and which we are currently considering, involves ‘mapping’ (1) onto a prototypical model proposed by Koper [11]; see also [3] for details.) We have sketched how the analysis of [12] can be adapted to the present context, which has allowed us to characterise the mixed-mode patterns that will ‘generically’ occur in (1), as well as to estimate the relevant parameter intervals. Recalling that the signature L^k encodes the segment consisting of k SAOs and L LAOs, and consulting Section 3.6 of [12], we may conclude that,

- (i) for $L = 1$, orbits contain segments of the form
 - (a) 1^k (possibly repeated some number of times),
 - (b) 1^{k-1} (possibly repeated some number of times), and
 - (c) 1^{k-2} , preceded by 1^k and followed by 1^{k-1} or 1^k ;
- (ii) for $L = 2$, only segments of the type 2^1 or 2^2 will occur;
- (iii) for $L \geq 2$, only segments of the form L^1 will be observed;

see Theorem 3.10, Proposition 3.11, and Corollary 3.12 of [12]. (For a detailed interpretation, and discussion, of the resulting mixed-mode dynamics, the reader is referred to [12, Section 4] and [13, Section IV].) The above predictions are supported by numerical simulation, which was performed in MAPLE for the parameter regime considered by Sekikawa *et al.* [18] – with $\varepsilon = 0.1$, $k_1 = 0.35$, and B_0 close to $\frac{1}{2}$ in (1) – under the additional assumption that $k_3 = 0.1 (= \varepsilon)$. (Specifically, we have simulated the corresponding transformed system of equations in (12) for values of μ close to μ^c , where we recall that $\kappa \equiv k_1$.) Throughout, we have set the initial condition to $(v, z, w)(0) = (0, 0, -0.01)$, unless explicitly stated otherwise; moreover, we have illustrated the resulting time series starting at time $t = 10^3$, after all transients have subsided.

As expected, we observe the unfolding of an entire family of non-trivial MMOs upon variation of the parameter μ : in Figure 9(a), we still have relaxation, while (periodic) orbits with signature L^1 for $L = 6, 4, 3$, and 2 – the latter two of which are separated by a ‘mixed’ pattern of the form $3^1 2^1$ – occur with decreasing μ , as shown in Figures 9(b) through 9(f).

Then, as μ is decreased further, a transition is observed towards $L = 1$, beginning with the $2^1 1^1$ -type pattern displayed in Figure 10(a). That pattern is followed by stable orbits of type 1^k , $k = 1, 2, \dots$, which are again interspersed with mixed patterns of the form $1^k(1^{k-1})^\ell$; see Figures 10(b) through 10(f) and Figures 11(a) through 11(f) for representative examples. (In fact, it follows from items (i) through (iii) above that the signatures 1^k and $1^k 1^{k-1}$ will dominate the mixed-mode dynamics of (1), with a transition that is roughly of the form $\dots \rightarrow 1^k \rightarrow 1^k 1^{k-1} \rightarrow 1^{k-1} \rightarrow \dots$, in accordance with our findings.) Finally, it is obvious from Figures 12(a) and 12(b) that the ‘highest’ 1^k -type pattern – at least with the chosen initial condition, and to the accuracy considered here – is achieved for $k = 8$, after which point pure SAO dynamics of type 0^1 takes over, in agreement with our claim that only a finite number of SAOs can occur in any given mixed-mode time series in (12).

Remark 6. Our numerics suggests that some variation in k_1 and k_3 does not qualitatively alter our conclusions on the mixed-mode dynamics of Equation (1) as long as the condition $k_3 = \mathcal{O}(\varepsilon)$ is satisfied; examples can be found in Figures 13(a) and 13(b). \square

While the above observations are of a qualitative nature, it is nevertheless possible to obtain some insight into the quantitative properties of the mixed-mode dynamics of Equation (12) from our analysis. On the basis of Proposition 5, one can thus show that, for each $k \geq 1$ and ε sufficiently small, the width of the μ -interval corresponding to stable 1^k -type dynamics will be of the order $\mathcal{O}[\sqrt{\varepsilon}(-\ln \varepsilon)^{-\frac{1}{2}}]$. Specifically, approximating the integral term in Equation (41) as in [12, Section 3.6], one finds

$$\Delta\mu^k = \frac{\underline{\mu}_k \kappa}{\sqrt{2} D_\mu} \frac{\sqrt{\varepsilon}}{\sqrt{-\ln \varepsilon}} [\ln(\sqrt{-\ln \varepsilon}) + \mathcal{O}(1)].$$

Evaluating the above estimate for $k_1(= \kappa) = 0.35$, $\varepsilon = 0.1$, and $\mu = \mu^c$ and noting that $D_\mu = 0.86625(= \frac{693}{800})$ then, we obtain $\Delta\mu^k \approx 0.00545[0.41702 + \mathcal{O}(1)]$, which agrees well with the corresponding numerical values of $\Delta\mu^k$ of about 0.004 to 0.005 that were inferred visually by simulating Equation (12) for varying values of μ , as above, and by recording the observed mixed-mode patterns. (The degree of agreement seems particularly encouraging given the ‘large’ value of $\varepsilon = 0.1$ considered here.) In sum, numerical simulation hence suggests that the μ -interval on which the mixed-mode dynamics of Equation (12) unfolds is approximately given by $(\underline{\mu}, \bar{\mu}) \approx (0.0465, 0.1125)$, which implies, in particular, $\Delta\mu \approx 0.0660$. Finally, it is worth noting that our numerical estimates for $\underline{\mu}$ and $\bar{\mu}$ satisfy $\mu^H < \underline{\mu} < \bar{\mu} < \mu^c$, as predicted. (Here, μ^H and μ^c are defined as at the beginning of Section 3.)

The parameter regime considered in this article motivated a simple scaling of k_3 with ε ; in fact, we set $k_3 = \varepsilon$. More generally, however, one could interpret k_3 – or even $k_1 k_3$ – as an effective small parameter that is independent of ε ; correspondingly, Equation (6) could then be studied as a true two-parameter singular perturbation problem. While geometric singular perturbation theory [6, 10] has matured as a field, however, the mathematics of such problems remains rudimentary; hence, we decided not to pursue that line of enquiry here. Still, further investigation into whether our results can be extended accordingly seems warranted, as preliminary analysis has revealed interesting dynamics in a similar generalisation of the canonical Equation (2). In particular, co-existence of mixed-mode oscillatory behaviour and delayed passage through Hopf bifurcation [15] has been observed, and will be elaborated on in an upcoming publication. Intuitively, such dynamics is due to a change in the strength of the global return mechanism: when $\varepsilon = \mathcal{O}(k_3)$, w is not necessarily

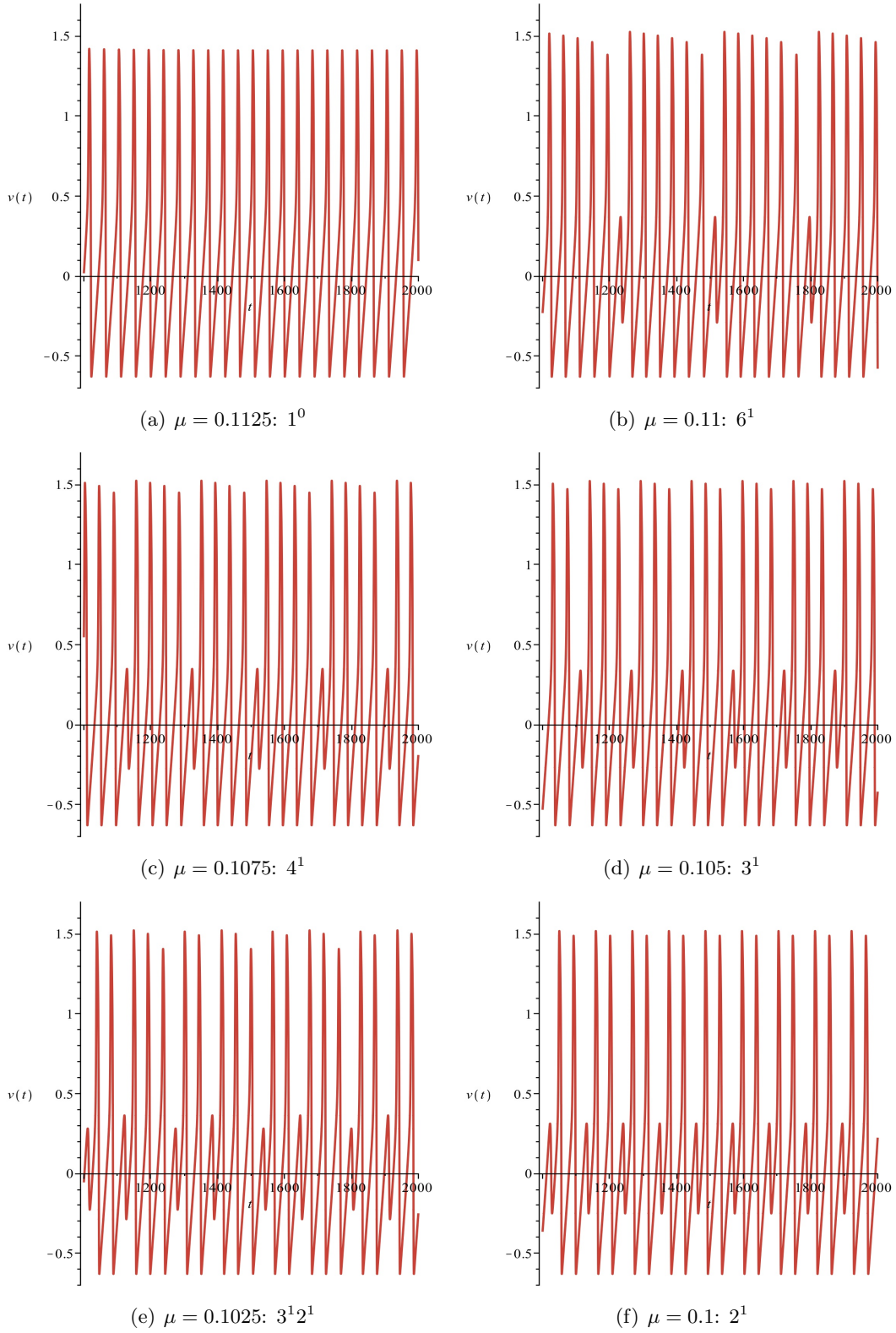


FIGURE 9. Mixed-mode dynamics of Equation (12) for varying values of μ .

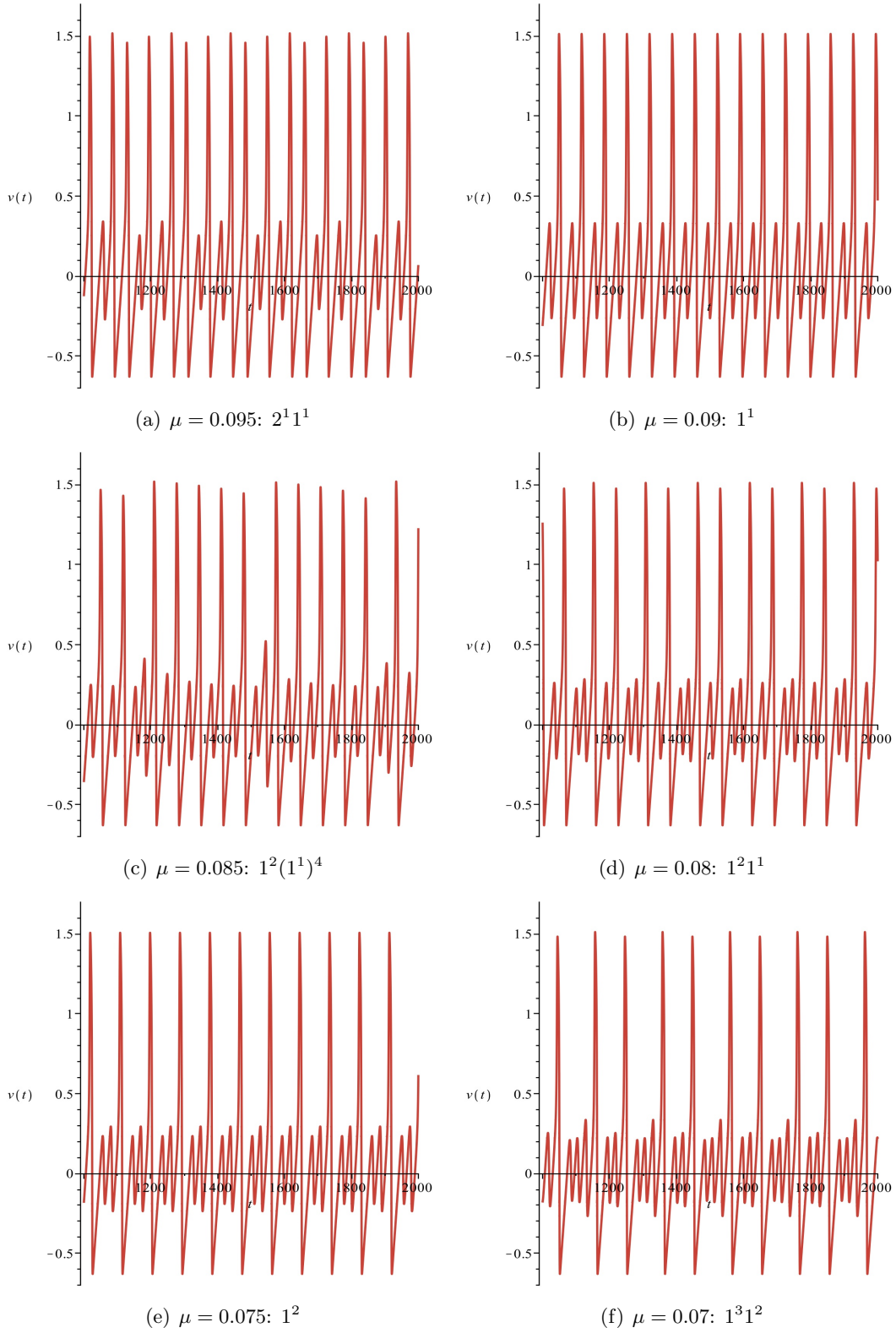


FIGURE 10. Mixed-mode dynamics of Equation (12) for varying values of μ .

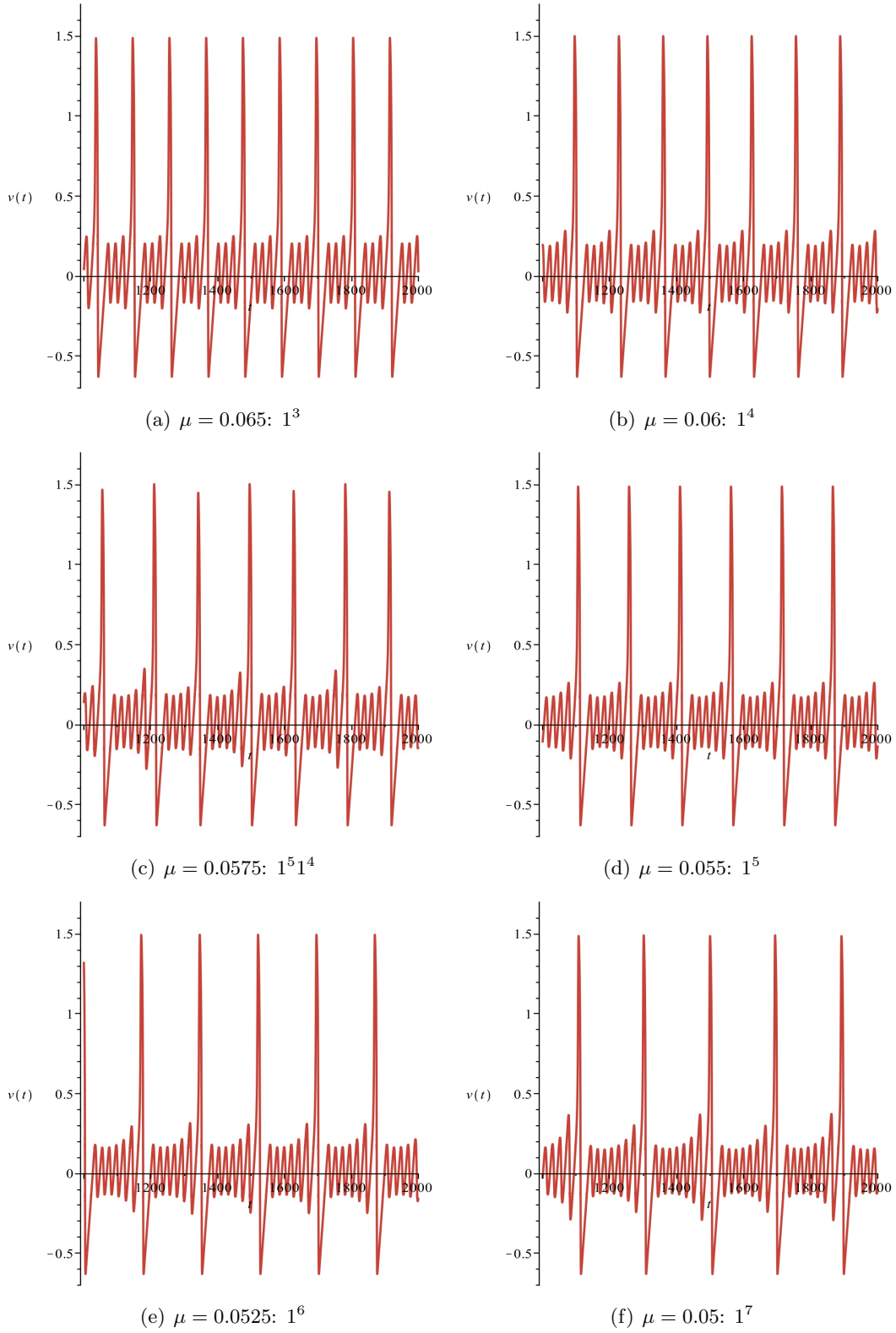


FIGURE 11. Mixed-mode dynamics of Equation (12) for varying values of μ .

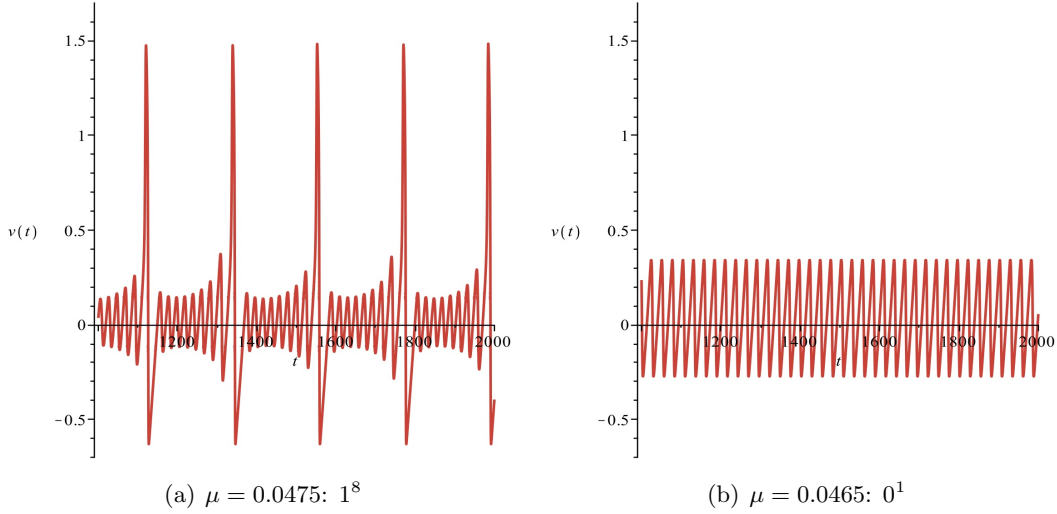


FIGURE 12. Mixed-mode dynamics of Equation (12) for varying values of μ .

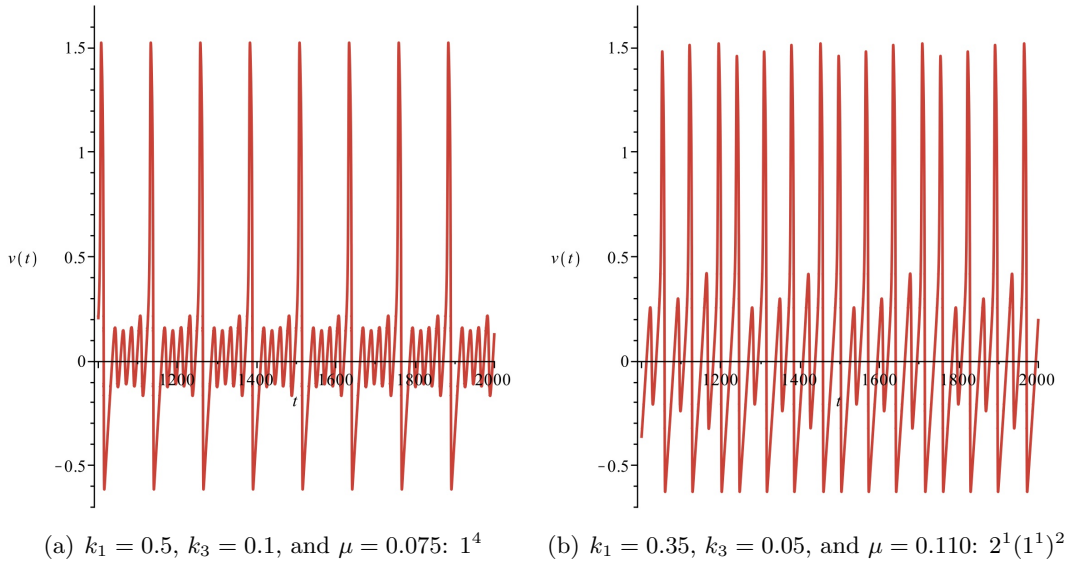


FIGURE 13. Effect of varying k_1 and k_3 on the dynamics of Equation (12).

reset to a neighbourhood of the strong canard Γ_ε ; rather, the corresponding return point may lie well away from the folded equilibrium P^+ in that case.

Remark 7. We note that we chose to fix the parameter k_1 , rather than to scale it with ε , as was also done in [18] – in spite of the fact that $k_1 = \mathcal{O}(\sqrt{\varepsilon})$. That choice complicates our analysis slightly, as it necessitates a correction to the return map $\bar{\Pi}$ in the fold region that was not present in [12]; recall the proof of Proposition 1. However, it seems in keeping with the assumptions made in [18]. \square

The ‘folded saddle-node of type II’ [20] uncovered in Equation (1) has also been studied in connection with a so-called ‘singular Hopf bifurcation;’ see [8] and the references therein for details.

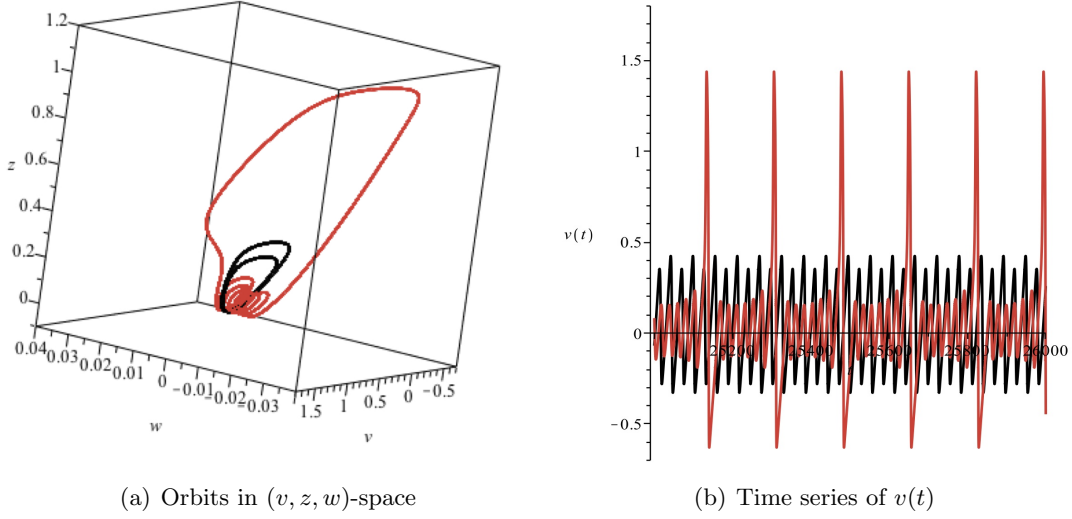


FIGURE 14. Co-existence of type-1⁶ MMO (red) and canard cycle after period doubling (black) for $\mu = 0.051$.

Roughly speaking, such bifurcations are observed in an ε -neighbourhood of a fold curve (for sufficiently small values of ε), and have been suggested as an alternative mechanism for generating mixed-mode dynamics; the relationship between folded saddle-node equilibria and singular Hopf bifurcation has been investigated in detail in [2]. In our case, it is straightforward to show that (1) has an equilibrium point at $P^* = (x_*, y_*, z_*)$, with $y_* = z_* = -\frac{1}{2}x_*(1 - x_*^2)$; following the procedure outlined in [8, Section 3.1], one can verify that P^* undergoes a Hopf bifurcation if the characteristic polynomial of the corresponding Jacobian,

$$\begin{aligned} \lambda^3 + \frac{1}{\varepsilon} [\varepsilon k_1(1 + k_3) - (1 - 3x_*^2)] \lambda^2 + \frac{1}{\varepsilon} [\varepsilon k_1^2 k_3 + (1 - k_1 + 3k_1 x_*^2)(1 + k_3)] \lambda + \frac{1}{\varepsilon} k_1 k_3 [2 - k_1(1 - 3x_*^2)] \\ \equiv \lambda^3 + a_2(x_*, k_1, k_3, \varepsilon) \lambda^2 + a_1(x_*, k_1, k_3, \varepsilon) \lambda + a_0(x_*, k_1, k_3, \varepsilon) = 0, \end{aligned}$$

satisfies $a_1 > 0$ and $a_1 a_2 = a_0$. The former condition holds in the parameter regime considered here, while the latter is met for the unique value $x_H \approx 0.56801$ of $x_* \equiv x_*(k_1, k_3, \varepsilon)$. Finally, solving for the corresponding B_0 -value in (1), we find $B_0^H \approx 0.50067$ which, incidentally, is equivalent to the value for μ^H obtained in Section 3, in the context of (11). (Similarly, one can show that the critical μ -value μ^c defined in Section 2.4 corresponds to $B_0^c = 0.26\sqrt{3} \approx 0.45488$ and, hence, that the mixed-mode dynamics of the three time-scale Bonhoeffer-van der Pol oscillator will unfold approximately over the interval (B_0^c, B_0^H) .) Since, however, the asymptotics obtained in this article is, by definition, only valid in an ‘intermediate’ μ -regime – away from both ‘pure’ SAO and LAO dynamics – we do not consider mixed-mode behaviour that may be induced by a singular Hopf bifurcation in (1).

While our analysis is mostly precise, as we have systematically accounted for the orders of any terms omitted in the process, a fully rigorous study would have to rely on the ‘blow-up’ technique, or geometric desingularisation [5, 14]. In fact, the discussion in Section 3.1 could equally be recast in terms of a ‘rescaling’ chart that covers the fold region and two ‘phase-directional’ charts which describe the entry and exit mechanisms, respectively, as is routinely done in the application of blow-up; see again [5, 14] for but two examples. However, in the interest of keeping

our presentation accessible, and in following [12] and [13], we have opted to formulate our results in terms of equivalent coordinate rescalings and projectivisations, and thereby to sacrifice some rigour.

Our approach has its inherent limitations, of course: thus, for instance, the asymptotics of the return map Π derived in Section 3 – as well as of its one-dimensional reduction Φ – breaks down at the boundaries between sectors of rotation; see [12, Section 4] for details. While we have hence excluded a neighbourhood of the corresponding secondary canards Γ_ε^j from our analysis, it is there that complicated mixed-mode patterns can arise due to ‘jumps’ between non-adjacent sectors and period-doubling bifurcation, both of which may yield chaotic dynamics. In fact, the proof of Proposition 1 already assumes that the flow of Equation (14) stays away from the strong canard Γ_ε , which is reflected in our assumption that $h = \mathcal{O}(\varepsilon^M)$ is small, but not exponentially so. Dynamics resulting from a violation of that condition is illustrated in Figure 14, where a stable mixed-mode pattern is shown to co-exist with a canard cycle undergoing period doubling; the latter is realised for initial w -values close to the ‘critical’ value $w_0^c = \sqrt{\varepsilon}\bar{w}_0^c$ of w , with \bar{w}_0^c defined as in (35), which implies that the corresponding h -value must be near-exponentially small.

Period-doubling in the extended Bonhoeffer-van der Pol oscillator has been studied in detail in [7]; in the process, the mixed-mode dynamics that is generated upon variation of the two parameters k_3 and B_0 was described numerically in a number of regimes, down to $k_3 = 0.2$. However, and in contrast to standard convention, mixed-mode patterns were organised in terms of ‘isospike diagrams,’ *i.e.*, distinguished in terms of the total number of ‘spikes’ within a period, rather than their signature L^k ; interestingly, it was shown that the underlying hierarchical structure is well-represented by a Stern-Brocot tree, instead of the Farey tree which is usually invoked in that context. In particular, and in agreement with [18], period-doubling cascades were found to be interspersed with chaotic phases which unfold over very narrow B_0 -intervals; the latter may well correspond to the boundaries between our sectors of rotation. Further investigation is necessary to establish fully how their results relate to those obtained in this article.

Finally, in a recent study by Shimizu *et al.* [19], the dynamics of a modification of Equation (1) was considered subject to a weak periodic perturbation close to Hopf bifurcation. In analogy to the approach developed here, a one-dimensional reduction was obtained for the return map that is induced by the resulting flow; however, that reduced map was not found to be unimodal, as in our case, but circle-like. A novel type of bifurcation, termed ‘MMO-incrementing bifurcation’ (MMOIB), was reported by the authors; moreover, highly complex, intermittently chaotic mixed-mode patterns that include rare bursts over long time intervals were observed in the corresponding time series. It would seem worthwhile to explore whether the geometric framework applied in this article can be extended to the modified Bonhoeffer-van der Pol oscillator studied in [19].

REFERENCES

- [1] M. Brøns, M. Krupa, and M. Wechselberger. Mixed mode oscillations due to the generalized canard phenomenon. In *Bifurcation theory and spatio-temporal pattern formation*, volume 49 of *Fields Inst. Commun.*, pages 39–63. Amer. Math. Soc., Providence, RI, 2006.
- [2] R. Curtu and J. Rubín. Interaction of canard and singular Hopf mechanisms in a neural model. *SIAM J. Appl. Dyn. Syst.*, 10(4):1443–1479, 2011.
- [3] M. Desroches, J. Guckenheimer, B. Krauskopf, C. Kuehn, H. M. Osinga, and M. Wechselberger. Mixed-mode oscillations with multiple time scales. *SIAM Rev.*, 54(2):211–288, 2012.
- [4] F. Dumortier. Techniques in the theory of local bifurcations: blow-up, normal forms, nilpotent bifurcations, singular perturbations. In *Bifurcations and periodic orbits of vector fields (Montreal, PQ, 1992)*, volume 408 of *NATO Adv. Sci. Inst. Ser. C Math. Phys. Sci.*, pages 19–73. Kluwer Acad. Publ., Dordrecht, 1993.
- [5] F. Dumortier and R. Roussarie. Canard cycles and center manifolds. *Mem. Amer. Math. Soc.*, 121(577):x+100, 1996. With an appendix by Cheng Zhi Li.
- [6] N. Fenichel. Geometric singular perturbation theory for ordinary differential equations. *J. Differential Equations*, 31(1):53–98, 1979.

- [7] J. G. Freire and J. A. C. Gallas. Stern-Brocot trees in cascades of mixed-mode oscillations and canards in the extended Bonhoeffer-van der Pol and the Fitzhugh-Nagumo models of excitable systems. *Phys. Lett. A*, 375:1097–1103, 2011.
- [8] J. Guckenheimer. Singular Hopf bifurcation in systems with two slow variables. *SIAM J. Appl. Dyn. Syst.*, 7(4):1355–1377, 2008.
- [9] E. M. Izhikevich. *Dynamical systems in neuroscience: the geometry of excitability and bursting*. Computational Neuroscience. MIT Press, Cambridge, MA, 2007.
- [10] C. K. R. T. Jones. Geometric singular perturbation theory. In *Dynamical systems (Montecatini Terme, 1994)*, volume 1609 of *Lecture Notes in Math.*, pages 44–118. Springer, Berlin, 1995.
- [11] M. T. M. Koper. Bifurcations of mixed-mode oscillations in a three-variable autonomous van der Pol-Duffing model with a cross-shaped phase diagram. *Phys. D*, 80(1-2):72–94, 1995.
- [12] M. Krupa, N. Popović, and N. Kopell. Mixed-mode oscillations in three time-scale systems: a prototypical example. *SIAM J. Appl. Dyn. Syst.*, 7(2):361–420, 2008.
- [13] M. Krupa, N. Popović, N. Kopell, and H. G. Rotstein. Mixed-mode oscillations in a three time-scale model for the dopaminergic neuron. *Chaos*, 18(1):015106, 19, 2008.
- [14] M. Krupa and P. Szmolyan. Extending geometric singular perturbation theory to nonhyperbolic points—fold and canard points in two dimensions. *SIAM J. Math. Anal.*, 33(2):286–314 (electronic), 2001.
- [15] M. Krupa and M. Wechselberger. Local analysis near a folded saddle-node singularity. *J. Differential Equations*, 248(12):2841–2888, 2010.
- [16] C. Kuehn. Personal communication, 2013.
- [17] F. W. J. Olver. *Asymptotics and special functions*. AKP Classics. A K Peters Ltd., Wellesley, MA, 1997. Reprint of the 1974 original [Academic Press, New York].
- [18] M. Sekikawa, N. Inaba, T. Yoshinaga, and Hikihara T. Period-doubling cascades of canards from the extended Bonhoeffer-van der Pol oscillator. *Phys. Lett. A*, 374(36):3745–3751, 2010.
- [19] K. Shimizu, S. Yuto, M. Sekikawa, and N. Inaba. Complex mixed-mode oscillations in a Bonhoeffer-van der Pol oscillator under weak periodic perturbation. *Phys. D*, 241(18):1518–1526, 2012.
- [20] P. Szmolyan and M. Wechselberger. Canards in \mathbb{R}^3 . *J. Differential Equations*, 177(2):419–453, 2001.
- [21] P. Szmolyan and M. Wechselberger. Relaxation oscillations in \mathbb{R}^3 . *J. Differential Equations*, 200(1):69–104, 2004.
- [22] S. T. Tu. A phase-plane analysis of bursting in the three-dimensional Bonhoeffer-van der Pol equations. *SIAM J. Appl. Math.*, 49(2):331–343, 1989.
- [23] M. Wechselberger. Existence and bifurcation of canards in \mathbb{R}^3 in the case of a folded node. *SIAM J. Appl. Dyn. Syst.*, 4(1):101–139 (electronic), 2005.
- [24] C. J. Wilson and J. C. Callaway. Coupled oscillator model of the dopaminergic neuron of the substantia nigra. *J. Neurophysiol.*, 83(5):3084–3100, 2000.

HASSELT UNIVERSITY, CAMPUS DIEPENBEEK, AGORALAAN GEBOUW D, B-3590 DIEPENBEEK, BELGIUM
E-mail address: Peter.DeMaesschalck@uhasselt.be

HASSELT UNIVERSITY, CAMPUS DIEPENBEEK, AGORALAAN GEBOUW D, B-3590 DIEPENBEEK, BELGIUM, AND
 AGH UNIVERSITY OF SCIENCE AND TECHNOLOGY, AL. MICKIEWICZA 30, 30-059 KRAKÓW, POLAND
E-mail address: Ekaterina.Kutafina@uhasselt.be

UNIVERSITY OF EDINBURGH, SCHOOL OF MATHEMATICS AND MAXWELL INSTITUTE FOR MATHEMATICAL SCIENCES,
 JAMES CLERK MAXWELL BUILDING, KING’S BUILDINGS, MAYFIELD ROAD, EDINBURGH EH9 3JZ, UNITED KINGDOM
E-mail address: Nikola.Popovic@ed.ac.uk